Transp Porous Med (2013) 100:159–192
DOI 10.1007/s11242-013-0210-6

Semi-Analytical Solutions for a Partially Penetrated Well with Wellbore Storage and Skin Effects in a Double-Porosity System with a Gas Cap

Morteza Dejam · Hassan Hassanzadeh · Zhangxin Chen

Received: 28 January 2013 / Accepted: 22 July 2013 / Published online: 2 August 2013

Abstract We have studied the effect of a constant top pressure on the pressure transient analysis of a partially penetrated well in an infinite-acting fractured reservoir with wellbore storage and skin factor effects. Semi-analytical solutions of a two-dimensional diffusivity equation have been obtained by using successive applications of the Laplace and modified finite Fourier sine transforms. Both pseudo-steady-state and transient exchanges between the matrix and the fractures have been considered. Solutions are presented that can be used to generate type curves for pressure transient analysis or can be used as a forward model in parameter estimation. The presented analysis has applications in well testing of fractured aquifers and naturally fractured oil reservoirs with a gas cap.

Keywords Infinite-acting · Double-porosity · Gas cap · Skin factor · Wellbore storage · Pressure transient analysis · Laplace transform · Modified finite Fourier sine transform · Fractured reservoirs

List of Symbols

A_1	First constant of general solution (85)
A_2	Second constant of general solution (85)
a_n	Function of the variable of the modified finite Fourier sine transform
B_o	Oil formation volume factor
c_{fo}	Fracture compressibility of the oil zone (LT^2/M)
c_{mo}	Matrix compressibility of the oil zone (LT^2/M)
C_s	Wellbore storage coefficient (L^4T^2/M)
C_{sD}	Dimensionless wellbore storage coefficient
$f(s)$	Function of the variable of the Laplace transform
h_D	Ratio of the perforated thickness to the total thickness of oil zone (i.e., dimensionless perforation interval)

M. Dejam · H. Hassanzadeh (✉) · Z. Chen
Department of Chemical and Petroleum Engineering, Schulich School of Engineering, University of Calgary, 2500 University Drive NW, Calgary, AB T2N 1N4, Canada
e-mail: hhassanz@ucalgary.ca

h_{m}	Thickness of the matrix block (L)
h_{o}	Total thickness of the oil zone (L)
h_{oD}	Dimensionless total thickness of the oil zone
h_{p}	Perforated thickness of the oil zone (L)
h_{pD}	Dimensionless perforated thickness of the oil zone
I_0	Modified Bessel function of the first kind of order 0
k_{fD}	Horizontal-to-vertical fracture permeability ratio
k_{fh}	Horizontal fracture permeability (L^2)
k_{fv}	Vertical fracture permeability (L^2)
k_{m}	Matrix permeability (L^2)
K_0	Modified Bessel function of the second kind of order 0
K_1	Modified Bessel function of the second kind of order 1
n	Variable of the modified finite Fourier sine transform
p_{f}	Fracture pressure ($\mathrm{M/LT}^2$)
p_{fD}	Dimensionless fracture pressure
$\bar{p}_{\mathrm{fD}}$	Dimensionless fracture pressure in the Laplace domain
$\tilde{\bar{p}}_{\mathrm{fD}}$	Modified finite Fourier sine transform of $\bar{p}_{fD}$
$p_{\mathrm{f,S}}$	Fracture pressure including skin effect ($\mathrm{M/LT}^2$)
$p_{\mathrm{fD,S}}$	Dimensionless fracture pressure including skin effect
p_{i}	Initial pressure in the oil zone of the fractured reservoir [$\mathrm{M/LT}^2$]
p_{m}	Matrix pressure ($\mathrm{M/LT}^2$)
$p_{\mathrm{m}D}$	Dimensionless matrix pressure
$\bar{p}_{\mathrm{mD}}$	Dimensionless matrix pressure in the Laplace domain
p_{wD}	Dimensionless average pressure response of the well
$\bar{p}_{\mathrm{wD}}$	Dimensionless average pressure at the wellbore in the Laplace domain
q_{o}	Oil flow rate (L^3/T)
r	Radius (L)
r_{D}	Dimensionless radius
r_{w}	Well radius (L)
r_{wD}	Dimensionless wellbore radius
s	Variable of the Laplace transform
S	Skin factor
S_{fo}	Fracture storativity of the oil zone ($\mathrm{L}^2\mathrm{T}^2/\mathrm{M}$)
S_{mo}	Matrix storativity of the oil zone ($\mathrm{L}^2\mathrm{T}^2/\mathrm{M}$)
S_{to}	Total storativity of the oil zone ($\mathrm{L}^2\mathrm{T}^2/M$)
t	Time (T)
t_{D}	Dimensionless time
z	Vertical direction in the oil zone of the fractured reservoir (L)
z_{m}	Vertical coordinate of the matrix block (L)
z_{D}	Dimensionless vertical direction in the oil zone of the fractured reservoir
z_{mD}	Dimensionless vertical coordinate of the matrix block

Greek Symbols

cos	Cosine
ln	Natural logarithm
$\ell_{t_{\mathrm{D}}}$	Laplace transform with respect to t_{D}
ℓ_s^{-1}	Inverse Laplace transform with respect to s
$\wp_{z_{\mathrm{D}}}$	Modified finite Fourier sine transform with respect to z_{D}

$\wp_n^{-1}$	Inverse modified finite Fourier sine transform with respect to n
ϕ_{fo}	Fracture porosity of the oil zone
ϕ_{mo}	Matrix porosity of the oil zone
η	Function of s and a_n
λ	Matrix–fracture interporosity flow coefficient
σ	Shape factor ($1/L^2$)
μ_{o}	Oil viscosity (M/LT)
ω	Storativity ratio

Subscripts

D	Dimensionless
f	Fracture
i	Initial
m	Matrix
n	Variable of the modified finite Fourier sine transform
o	Oil
p	Perforated
s	Storage
s	Variable of the Laplace transform
S	Skin
t_{D}	Dimensionless time
w	Well
z_{D}	Dimensionless vertical direction
0,1	Orders 0 and 1 for modified Bessel functions of the first and second kinds
1,2	First and second constants of the general solution (85)

Superscripts

$-$	Laplace transform
-1	Inverse of Laplace transform or modified finite Fourier sine transform
$\sim$	Modified finite Fourier sine transform

1 Introduction

A major portion of the world's water resources and hydrocarbon reserves exist in fractured formations. Fractured rocks are modeled by considering two media: the fractures and the rock matrix. Usually, fractures are highly conductive, with low storage capacity. On the other hand, a rock matrix has low permeability and high storage capacity.

Double-porosity and double-permeability models are widely used to model fluid flow and transport through fractured porous media in hydrological sciences and petroleum reservoir applications. In a double-permeability model, adjacent matrix blocks communicate with each other; and, in a double-porosity model, adjacent matrix blocks do not communicate. The double-porosity model considers a simple idealization of fractured formations in which the fractures are uniform and well connected, while the rock matrix is composed of a stack of equally sized blocks (sugar-cube model).

Based on the theory developed in the early 1960s by Barenblatt et al. (1960); Warren and Root (1963) introduced the concept of a double-porosity model into petroleum reservoir applications. They applied the double-porosity concept to model the wellbore pressure

response of infinite-acting, naturally fractured reservoirs by presenting an analytical solution for single-phase, unsteady-state flow in these reservoirs. They utilized a pseudo-steady-state formulation for the matrix-to-fracture flow in their model. A pseudo-steady-state indicates that the mass transfer between the matrix and the fractures is proportional to their pressure difference.

Saidi (1983) suggested that when a fractured porous medium is composed of relatively large matrix blocks and/or it is under a relatively large rate of pressure reduction, the pseudo-steady-state assumption for the matrix–fracture exchange term causes large errors in the simulation of naturally fractured reservoirs compared to the transient pressure condition.

Warren and Root (1963) described the wellbore pressure response with two main parameters: the interporosity flow coefficient and the storativity ratio. The interporosity flow coefficient, λ, is proportional to the ratio of matrix permeability to fracture permeability and typically varies from 10^{-3} to 10^{-9}. Lower values of the interporosity flow coefficient show lower fluid transfer between the matrix and the fracture. The storativity ratio, ω, is a dimensionless parameter and is defined as the fluid capacitance of the fractures divided by that of the total system. A semi-log plot of wellbore pressure response versus time for the Warren and Root (1963) model yielded a characteristic *S*-shaped curve with an inflection point. The separation of the two parallel lines allows for the calculation of the storativity ratio. As $\omega \longrightarrow 1$ or $\lambda \longrightarrow \infty$ in a double-porosity model, the behavior of a fractured reservoir approaches that of an equivalent system of an ordinary porous reservoir.

The subject of pressure transient analysis of double-porosity reservoirs has been studied extensively in the literature (Kazemi 1969; Gringarten and Ramey 1973; de Swaan 1976; Najurieta 1980; Serra et al. 1983; Streltsova 1983; Moench 1984; Chen 1989; Chen et al. 1991; Zimmerman et al. 1993; Hamm and Bidaux 1996; Slimani and Tiab 2008; De Smedt 2011; Nie et al. 2012; Yao et al. 2012; Biryukov and Kuchuk 2012; Jia et al. 2013). A detailed review of previous works is given elsewhere (Hassanzadeh et al. 2009).

The results of pressure transient tests may be affected by two important parameters: the skin factor and the wellbore storage coefficient. The skin factor describes the damage or stimulation effects near the wellbore, and wellbore storage causes a delay in the fluid transport from the formation to the well (Sabet 1991). The early period region of pressure transient tests is usually dominated by wellbore storage (Sabet 1991).

The impacts of the skin factor and wellbore storage coefficient on the results of well tests have been widely investigated (van Everdingen and Hurst 1949; van Everdingen 1953; Hawkins 1956; Agarwal et al. 1970; Wattenbarger and Ramey 1970; Ramey and Agarwal 1972; Earlougher and Kersch 1974; Bilhartz and Ramey 1977; Sandal et al. 1978; Tariq and Ramey 1978; Bourdet and Gringarten 1980; Buhidma and Raghavan 1980; Chu et al. 1984; Moench 1984, 1985; Abdassah and Ershaghi 1986; Jalali and Ershaghi 1987; Hamm and Bidaux 1996; Yang and Gates 1997; Cassiani et al. 1999; Kabala 2001; Lods and Gouze 2004; Pasandi et al. 2008; Sethi 2011). Agarwal et al. (1970) modified the boundary condition at the well radius to include the effects of the wellbore storage coefficient and skin factor and conducted a fundamental study of the importance of these two parameters on short-term transient flow. The effects of these two parameters on the results of pumping tests in groundwater have been extensively studied (Moench 1984, 1985; Hamm and Bidaux 1996; Yang and Gates 1997; Cassiani et al. 1999; Kabala 2001; Lods and Gouze 2004; Pasandi et al. 2008; Sethi 2011). Pasandi et al. (2008) developed a mathematical model incorporating the impacts of partial penetration, wellbore storage, anisotropy, finite- radius well skin, and non-instantaneous release of water from an unsaturated zone to describe groundwater flow in phreatic aquifers with two regions of radial flow in response to a constant-rate pumping test in single-porosity reservoirs.

The influences of the skin factor and wellbore storage coefficient are also applicable to pressure transient analysis of oil and gas wells (van Everdingen and Hurst 1949; van Everdingen 1953; Hawkins 1956; Agarwal et al. 1970; Wattenbarger and Ramey 1970; Ramey and Agarwal 1972; Earlougher and Kersch 1974; Bilhartz and Ramey 1977; Sandal et al. 1978; Tariq and Ramey 1978; Bourdet and Gringarten 1980; Buhidma and Raghavan 1980; Chu et al. 1984; Abdassah and Ershaghi 1986; Jalali and Ershaghi 1987). During oil production from naturally fractured petroleum reservoirs, the released gas in the fractures quickly segregates before arriving at the producing wells; most of it joins the expanding original gas cap or creates a secondary gas cap if no original gas cap is present (Peaceman 1976; Saidi 1987). There have been a limited number of studies on the effect of a gas cap on the pressure transient response of fractured formations.

Streltsova 1979 developed a technique to analyze the pressure transient response for a well with limited flow entry producing from three types of single-porosity oil reservoirs: an oil reservoir with a gas cap, an oil reservoir with gas–oil contact in a zone of low permeability, and an oil reservoir with impermeable top and bottom boundaries. In these two-dimensional (2D) models, it was assumed that the well was partially penetrated in an anisotropic reservoir with a gas cap overlying the oil zone. Streltsova (1979) considered a vertical flow in the upper low-permeability zone, including a gas cap that was assumed to be proportional to the pressure drawdown across this zone. The pseudo-skin factor was derived, due to limited flow entry, for the three types of oil reservoirs.

Streltsova (1981) extended the previous work (Streltsova 1979) and investigated the gas cap effect on the results of pressure buildup tests for wells producing from a single-porosity oil reservoir. Again, in this 2D model, a partially penetrated well was assumed to be in an anisotropic reservoir with a gas cap overlying the oil zone. Streltsova considered constant pressure at the gas–oil contact. In this work, wellbore storage and skin effects were included. Streltsova concluded that the gas cap modifies the middle-period region of pressure curves in a manner such that customary pressure buildup analysis cannot be utilized. In addition, Streltsova (1981) showed that, for a damaged well, the combined effects of the gas cap, wellbore storage, and skin factor make the analysis of a pressure buildup test very difficult and, in some cases, impossible. Buhidma and Raghavan (1980) used a 2D model to examine the characteristics of the wellbore pressure response versus time curves for a partially penetrating well located at the center of an anisotropic single-porosity reservoir and subject to constant pressure at bottom boundary (bottom water drive). They also investigated the influences of the penetration ratio and reservoir anisotropy on the transient behavior of the system. As a result, Buhidma and Raghavan (1980) demonstrated that the semi-log straight line reflecting the pseudoradial flow period is not observed if a constant pressure boundary exists at the bottom of the reservoir.

Dougherty and Babu (1984) developed a Laplace domain solution for flow to a partially penetrated well in a double-porosity reservoir. Their solutions to slug test problems show that the head response due to fractures is distinct from the response due to partial penetration or skin effect. Their results may be applicable to testing numerical models of flow in fractured porous media. Chu et al. (1984) discussed about the combined effects of skin factor, wellbore storage coefficient, partially penetrated well, and gas cap or bottom water aquifer (constant pressure at top or bottom boundary) on the analysis of pressure data in an anisotropic single-porosity reservoir using a 2D model. They demonstrated that for small values of the dimensionless wellbore storage coefficient and large values of dimensionless well length, the flow capacity of the perforated interval and the skin factor can be determined from data influenced by wellbore storage using the wellbore storage type curves (the full penetration solutions) available in the literature like Earlougher and Kersch (1974). Chu

et al. (1984) also mentioned that for other cases, the flow capacity of the entire interval and the total skin factor can be estimated again using the wellbore storage type curves (the full penetration solutions) available in the literature like Earlougher and Kersch (1974) if both (top and bottom) boundaries are sealed. Moreover, Chu et al. (1984) stated that in the case of existence of a constant pressure (gas cap or bottom water drive) at one of the boundaries, the solution presented in their work can be used.

Ozkan and Raghavan (1991a) derived point-source solutions in a Laplace-transform domain to calculate pressure distributions and well responses for a wide variety of wellbore configurations: partially penetrated vertical wells, horizontal wells, and fractured wells (complete or limited entry). They presented analytical solutions of a partially penetrated well in dual-porosity reservoirs with different combinations of top and bottom boundaries. The combination of a constant pressure boundary at the top and an impermeable boundary at the bottom represents the same geological model as shown in this paper. Ozkan and Raghavan (1991b) discussed computational considerations in presenting well pressure response for several cases developed in their previous work. Ozkan and Raghavan (1991b) used the equation presented by van Everdingen and Hurst (1949) to study the pressure response of a well with skin factor and wellbore storage-coefficient. However, their approach to solve flow equations is mathematically different than our work.

Al-Bemani and Ershaghi (1997) studied the gas cap effect on the pressure transient response for a well producing from a double-porosity reservoir that was composed of anisotropic fractures with a constant vertical-to-horizontal permeability ratio and isotropic matrix blocks. In this unsteady-state 2D model, the producing well was assumed to be fully penetrated along the oil zone and overlain by a gas cap. Moreover, the naturally fractured porous medium was considered to be infinite in the radial direction.

Al-Bemani and Ershaghi (1997) applied both the pseudo-steady-state and transient formulations for the matrix–fracture exchange term. They used a combination of the averaged pressure method in the vertical direction and the vertical linear flux boundary condition at the gas–oil contact in fractures to simplify a 2D equation. The solutions for the simplified model in a Laplace domain were converted to real-time using a numerical Laplace inversion method. They showed that when the gas cap effect commenced, the fracture or the matrix–fracture response deviated.

Al-Bemani and Ershaghi (1997) also showed that unusual slope changes during the transition period depended on the difference between the fracture anisotropy parameter (which is proportional to the vertical-to-horizontal fracture permeability ratio) and the matrix–fracture interporosity flow coefficient and also on the difference between the gas cap storativity ratio and the oil zone matrix storativity ratio.

Bui et al. (2000) presented an analytical solution that describes transient pressure behavior of partially penetrated wells in naturally fractured reservoirs. Their solution was obtained by combining a pseudo-steady-state model for naturally fractured reservoirs with a partially penetrated well model in homogeneous reservoirs. They generated new type curves from the analytical solution, which indicates that partial penetration and double-porosity effects cause a characteristic shape of the curves at early and transition times.

Fuentes-Cruz et al. (2004) obtained the pressure transient behavior for partially penetrated wells completed in naturally fractured–vuggy reservoirs by combination of Laplace transformation with respect to time and finite Fourier transformation with respect to vertical distance. They performed numerical Laplace inversion using the Stehfest (1970) algorithm. It should be mentioned that the approach used by Fuentes-Cruz et al. (2004) to obtain solutions is mathematically different from ours. Moreover, they did not include skin factor and wellbore storage-coefficient in their boundary conditions. In addition, they used the pseudo-

steady-state formulation for the matrix–fracture exchange term in their triple porosity model, while we used both pseudo-steady-state and transient formulations for the matrix–fracture exchange term in our double-porosity model.

The same work was done by Chen et al. (2008). They obtained the analytical solution of a partially perforated well in dual-porosity reservoirs with a gas cap by using the Laplace transformation and separation of variables methods.

In this work, we have investigated the pressure transient behavior of a partially penetrated well in an infinite-acting double-porosity system with a constant pressure at the top boundary, based on a semi-analytical solution of the 2D diffusivity equation using the Laplace and modified finite Fourier sine transforms. In addition, we have considered both pseudo-steady-state and transient formulations for the matrix–fracture exchange term. The presented analysis has applications in the flow of slightly compressible fluids in naturally fractured reservoirs with a gas cap.

This paper is organized as follows: first, the mathematical model and solutions are presented. Then the results are discussed, followed by a summary and conclusions.

2 Model Description and Solutions

2.1 Assumptions and Description of the Physical Model

We consider a 2D double-porosity system composed of continuous anisotropic fractures with a constant vertical-to-horizontal permeability ratio (k_{fv}/k_{fh}) and homogeneous isotropic matrix blocks (see Fig. 1). The fractured formation consists of an oil zone, which is a producing zone, with a thickness of h_o overlain by a gas cap with a thickness of h_g. The top boundary of the oil zone, where the gas–oil contact is located, is assumed to have constant pressure, and the bottom boundary of the oil zone is impermeable. The former assumption can be justified, since the gas compressibility is high compared to that of oil and the gas cap pressure remains fairly constant during a pressure transient test. The vertical direction is chosen to be downward with its origin at the gas–oil contact ($z = 0$). Darcy's law is considered applicable to the fluid flow in the matrix as well as in the fractures. The double-porosity system is considered as an infinite-acting reservoir in the radial direction. Due to

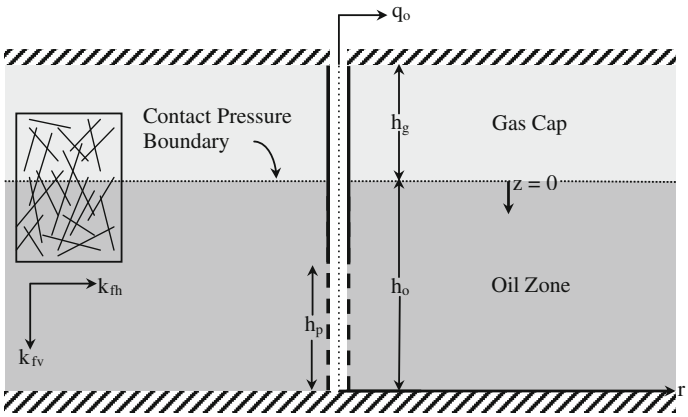

Fig. 1 A partially penetrated well in an oil zone overlain by a gas cap in a double-porosity system

short period of well test operation, the gas cap is assumed to be stationary or the gas–oil contact remains fixed and therefore the gravitational force can be ignored during well test operation.

The fluid flowing through the oil zone of the fractured reservoir is assumed to be a single phase, slightly compressible and with constant viscosity. A completed well of radius, r_w, is partially penetrated with a perforation interval, h_p, in the oil zone. The well produces at a constant flow rate, q_o.

We consider two different exchange rate formulations between the matrix and the fractures for production from a partially penetrated well in an infinite-acting double-porosity reservoir: pseudo-steady and transient.

2.2 Governing Equations

The governing 2D diffusivity equation that describes the pressure behavior in the oil zone of the fractured reservoir can be given by:

$$\frac{\partial^2 p_f(r,z,t)}{\partial r^2}+\frac{1}{r}\frac{\partial p_f(r,z,t)}{\partial r}+\frac{k_{fv}}{k_{fh}}\frac{\partial^2 p_f(r,z,t)}{\partial z^2} = \frac{\mu_o}{k_{fh}}\left[(\phi c)_{fo}\frac{\partial p_f(r,z,t)}{\partial t}+(\phi c)_{mo}\frac{\partial p_m(z_m,t)}{\partial t}\right] \tag{1}$$

where p_f and p_m are the fracture and matrix pressures, respectively; r is the radius; z is the vertical direction in the oil zone of the fractured reservoir; z_m is the vertical coordinate of the matrix block; t is the time; k_{fh} is the horizontal fracture permeability; k_{fv} is the vertical fracture permeability; μ_o is the oil viscosity; ϕ_{fo} is the fracture porosity; ϕ_{mo} is the matrix porosity; c_{fo} is the fracture compressibility; and c_{mo} is the matrix compressibility.

To solve Eq. (1), one initial condition, two boundary conditions in the r direction and two boundary conditions in the z direction are needed. The initial condition is:

$$p_f(r,z,0)=p_m(z_m,0)=p_i \tag{2}$$

where p_i is the initial pressure in the oil zone of the fractured reservoir.

Combination of Eq. (3) for non-perforated interval and Eq. (4) for perforated interval, which includes the effects of the wellbore storage-coefficient (C_s) and skin factor (S), is used as the inner boundary condition ($r=r_w$):

$$\left(\frac{\partial p_f(r,z,t)}{\partial r}\right)_{r=r_w}=0 \qquad 0<z<h_o-h_p \tag{3}$$

$$\begin{cases} p_{f,S}(r_w,z,t)=\left[p_f(r,z,t)-r_w\frac{h_p}{h_o}\left(\frac{\partial p_f(r,z,t)}{\partial r}\right)S\right]_{r=r_w} \\ q_oB_o=\frac{2\pi k_{fh}h_pr_w}{\mu_o}\left(\frac{\partial p_f(r,z,t)}{\partial r}\right)_{r=r_w}-C_s\frac{\partial p_{f,S}(r_w,z,t)}{\partial t} \end{cases} \qquad h_o-h_p<z<h_o \tag{4}$$

where $p_{f,S}$ is the fracture pressure including the skin effect, h_o is the total thickness of the oil zone, h_p is the perforated thickness of the oil zone, q_o is the oil flow rate, and B_o is the formation volume factor.

For a double-porosity system with infinite-acting behavior, the outer boundary condition ($r\longrightarrow+\infty$) is given by:

$$p_f(+\infty,z,t)=p_i \tag{5}$$

The respective boundary conditions at the top ($z = 0$) and bottom ($z = h_o$) of the oil zone of the infinite-acting fractured reservoir are written as follows:

$$p_f(r, 0, t) = p_i \tag{6}$$

$$\frac{\partial p_f(r, h_o, t)}{\partial z} = 0 \tag{7}$$

The fracture pressure at the gas–oil contact ($z = 0$) is assumed to remain fixed and equal to the initial pressure, p_i, during well test operation.

In order to make Eqs. (1–7) dimensionless, the following dimensionless variables are defined:

$$S_{fo} = (\phi c)_{fo} h_o \tag{8}$$

$$S_{mo} = (\phi c)_{mo} h_o \tag{9}$$

$$S_{to} = [(\phi c)_{fo} + (\phi c)_{mo}] h_o = S_{fo} + S_{mo} \tag{10}$$

$$p_{fD}(r_D, z_D, t_D) = \frac{2\pi k_{fh} h_o [p_i - p_f(r, z, t)]}{q_o \mu_o B_o} \tag{11}$$

$$p_{mD}(z_{mD}, t_D) = \frac{2\pi k_{fh} h_o [p_i - p_m(z_m, t)]}{q_o \mu_o B_o} \tag{12}$$

$$t_D = \frac{k_{fh} t}{[(\phi c)_{fo} + (\phi c)_{mo}] \mu_o r_w^2} \tag{13}$$

$$\omega = \frac{S_{fo}}{S_{to}} \tag{14}$$

$$k_{fD} = \frac{k_{fh}}{k_{fv}} \tag{15}$$

$$r_D = \frac{r}{r_w} \sqrt{\frac{1}{k_{fD}}} \tag{16}$$

$$z_D = \frac{z}{r_w} \tag{17}$$

$$z_{mD} = \frac{z_m}{\left(\frac{h_m}{2}\right)} \tag{18}$$

$$C_{sD} = \frac{C_s}{2\pi h_o [(\phi c)_{fo} + (\phi c)_{mo}] r_w^2} = \frac{C_s}{2\pi S_{to} r_w^2} \tag{19}$$

$$h_{oD} = \frac{h_o}{r_w} \tag{20}$$

$$h_{pD} = \frac{h_p}{r_w} \tag{21}$$

$$h_D = \frac{h_{pD}}{h_{oD}} = \frac{h_p}{h_o} \tag{22}$$

where S_{fo}, S_{mo}, and S_{to} are the fracture, matrix, and total storativities of the oil zone, respectively; p_{fD} and p_{mD} are the dimensionless fracture and matrix pressures, respectively; k_{fD} is the horizontal-to-vertical fracture permeability ratio; r_D is the dimensionless radius; z_D is the dimensionless vertical direction in the oil zone of the fractured reservoir; z_{mD} is the dimensionless vertical coordinate of the matrix block; h_m is the thickness of the matrix block; t_D is the dimensionless time; ω is the storativity ratio; C_{sD} is the dimensionless wellbore storage-coefficient; h_{oD} is the dimensionless total thickness of the oil zone; h_{pD} is the dimensionless

perforated thickness of the oil zone; and h_{D} is the ratio of the perforated thickness to the total thickness of the oil zone (i.e., dimensionless perforation interval).

By using the dimensionless variables listed in (8–22), the dimensionless forms of Eq. (1), the initial condition (2) and the boundary conditions (3–7) become, respectively:

$$\frac{\partial^2 p_{\mathrm{fD}}(r_{\mathrm{D}}, z_{\mathrm{D}}, t_{\mathrm{D}})}{\partial r_{\mathrm{D}}^2} + \frac{1}{r_{\mathrm{D}}}\frac{\partial p_{\mathrm{fD}}(r_{\mathrm{D}}, z_{\mathrm{D}}, t_{\mathrm{D}})}{\partial r_{\mathrm{D}}} + \frac{\partial^2 p_{\mathrm{fD}}(r_{\mathrm{D}}, z_{\mathrm{D}}, t_{\mathrm{D}})}{\partial z_{\mathrm{D}}^2} = k_{\mathrm{fD}}\left[\omega\frac{\partial p_{\mathrm{fD}}(r_{\mathrm{D}}, z_{\mathrm{D}}, t_{\mathrm{D}})}{\partial t_{\mathrm{D}}} + (1-\omega)\frac{\partial p_{\mathrm{mD}}(z_{\mathrm{mD}}, t_{\mathrm{D}})}{\partial t_{\mathrm{D}}}\right] \tag{23}$$

$$p_{\mathrm{fD}}(r_{\mathrm{D}}, z_{\mathrm{D}}, 0) = p_{\mathrm{mD}}(z_{\mathrm{mD}}, 0) = 0 \tag{24}$$

$$\left(\frac{\partial p_{\mathrm{fD}}(r_{\mathrm{D}}, z_{\mathrm{D}}, t_{\mathrm{D}})}{\partial r_{\mathrm{D}}}\right)_{r_{\mathrm{D}}=r_{\mathrm{wD}}} = 0 \quad 0 < z_{\mathrm{D}} < h_{\mathrm{oD}} - h_{\mathrm{pD}} \tag{25}$$

$$\begin{cases} p_{\mathrm{fD,S}}(r_{\mathrm{wD}}, z_{\mathrm{D}}, t_{\mathrm{D}}) = \left[p_{\mathrm{fD}}(r_{\mathrm{D}}, z_{\mathrm{D}}, t_{\mathrm{D}}) - h_{\mathrm{D}}\left(\frac{\partial p_{\mathrm{fD}}(r_{\mathrm{D}}, z_{\mathrm{D}}, t_{\mathrm{D}})}{\partial r_{\mathrm{D}}}\right) S\right]_{r_{\mathrm{D}}=r_{\mathrm{wD}}} \\ C_{\mathrm{sD}}\frac{\partial p_{\mathrm{fD,S}}(r_{\mathrm{wD}}, z_{\mathrm{D}}, t_{\mathrm{D}})}{\partial t_{\mathrm{D}}} - h_{\mathrm{D}}\left(\frac{\partial p_{\mathrm{fD}}(r_{\mathrm{D}}, z_{\mathrm{D}}, t_{\mathrm{D}})}{\partial r_{\mathrm{D}}}\right)_{r_{\mathrm{D}}=r_{\mathrm{wD}}} = 1 \end{cases}$$

$$h_{\mathrm{oD}} - h_{\mathrm{pD}} < z_{\mathrm{D}} < h_{\mathrm{oD}} \tag{26}$$

$$p_{\mathrm{fD}}(+\infty, z_{\mathrm{D}}, t_{\mathrm{D}}) = 0 \tag{27}$$

$$p_{\mathrm{fD}}(r_{\mathrm{D}}, 0, t_{\mathrm{D}}) = 0 \tag{28}$$

$$\frac{\partial p_{\mathrm{fD}}(r_{\mathrm{D}}, h_{\mathrm{oD}}, t_{\mathrm{D}})}{\partial z_{\mathrm{D}}} = 0 \tag{29}$$

where $p_{\mathrm{fD,S}}$ is the dimensionless fracture pressure, including the skin effect, and r_{wD} is the dimensionless wellbore radius, determined by $r_{\mathrm{wD}} = \sqrt{1/k_{\mathrm{fD}}}$.

The Laplace and modified finite Fourier sine transforms with respect to t_{D} and z_{D} are used to solve Eq. (23) accompanied with the initial condition (24) and boundary conditions (25–29). The details of the derivations are presented in Appendix.

The dimensionless average pressure response of the well (p_{wD}) and its derivative ($dp_{\mathrm{wD}}/d\ln t_{\mathrm{D}}$) in the oil zone of the infinite-acting double-porosity reservoir with a gas cap, including wellbore storage and skin factor effects, are obtained as:

$$p_{\mathrm{wD}}(t_{\mathrm{D}}) = \ell_{\mathrm{s}}^{-1}\left\{\frac{1}{h_{\mathrm{pD}}}\sum_{n=1}^{+\infty}\left[\frac{\frac{4}{\pi(2n-1)}\left[K_0(\eta r_{\mathrm{wD}}) + Sh_{\mathrm{D}}\eta K_1(\eta r_{\mathrm{wD}})\right]\cos\left[\left(\frac{2n-1}{2}\right)(1-h_{\mathrm{D}})\,\pi\right]}{sa_n\left[sC_{\mathrm{sD}}\left[K_0(\eta r_{\mathrm{wD}}) + Sh_{\mathrm{D}}\eta K_1(\eta r_{\mathrm{wD}})\right] + h_{\mathrm{D}}\eta K_1(\eta r_{\mathrm{wD}})\right]}\right]\right\} \tag{30}$$

$$\frac{dp_{\mathrm{wD}}(t_{\mathrm{D}})}{d\ln t_{\mathrm{D}}} = t_{\mathrm{D}}\ell_{\mathrm{s}}^{-1}\left\{\frac{1}{h_{\mathrm{pD}}}\sum_{n=1}^{+\infty}\left[\frac{\frac{4}{\pi(2n-1)}\left[K_0(\eta r_{\mathrm{wD}}) + Sh_{\mathrm{D}}\eta K_1(\eta r_{\mathrm{wD}})\right]\cos\left[\left(\frac{2n-1}{2}\right)(1-h_{\mathrm{D}})\,\pi\right]}{a_n\left[sC_{\mathrm{sD}}\left[K_0(\eta r_{\mathrm{wD}}) + Sh_{\mathrm{D}}\eta K_1(\eta r_{\mathrm{wD}})\right] + h_{\mathrm{D}}\eta K_1(\eta r_{\mathrm{wD}})\right]}\right]\right\} \tag{31}$$

where "s" is the variable of the Laplace transform; ℓ_{s}^{-1} is the inverse Laplace transform operator; n is the variable of the modified finite Fourier sine transform; K_0 and K_1 are modified Bessel functions of the second kind of order 0 and 1, respectively; and a_n is a function of the variable of the modified finite Fourier sine transform, determined by:

$$a_n = \left(n - \frac{1}{2}\right)\frac{\pi}{h_{\mathrm{oD}}}, \qquad n = 1, 2, 3, \ldots \tag{32}$$

and η is a function of "s" and a_n, defined as:

$$\eta = \sqrt{a_n^2 + k_{\mathrm{fD}} s f(\mathrm{s})} \tag{33}$$

where $f(\mathrm{s})$ for the pseudo-steady-state matrix–fracture exchange is presented by (Warren and Root 1963):

$$f(s) = \omega + \frac{(1-\omega)\lambda}{\lambda + (1-\omega)\mathrm{s}} \tag{34}$$

and $f(\mathrm{s})$ for the transient matrix–fracture exchange, assuming a slab-shaped matrix block, is given by (Serra et al. 1983; Ozkan et al. 1987; Stewart and Asharsobbi 1988; Da Prat 1990; Sabet 1991; Al-Bemani and Ershaghi 1997; Hassanzadeh et al. 2009):

$$f(\mathrm{s}) = \omega + \sqrt{\frac{\lambda(1-\omega)}{3\mathrm{s}}} \tanh\left(\sqrt{\frac{3(1-\omega)\mathrm{s}}{\lambda}}\right) \tag{35}$$

where λ is the matrix–fracture interporosity flow coefficient, defined as (Warren and Root 1963):

$$\lambda = \sigma \frac{r_{\mathrm{w}}^2 k_{\mathrm{m}}}{k_{\mathrm{fh}}} \tag{36}$$

where σ is the matrix–fracture transfer coefficient or the so-called shape factor, and k_{m} is the matrix permeability.

The $f(\mathrm{s})$ expression for the pseudo-steady state matrix-fracture exchange, Eq. (34), can be obtained by finding the relation between $\bar{p}_{\mathrm{fD}}(r_{\mathrm{D}}, z_{\mathrm{D}}, \mathrm{s})$ and $\bar{p}_{\mathrm{mD}}(z_{\mathrm{mD}}, \mathrm{s})$, Eq. (54), through Laplace solution of following governing equation, Eq. (37), along with the suitable initial condition, Eq. (24), for pseudo-steady-state pressure change inside the matrix block (Warren and Root 1963):

$$(1-\omega)\frac{\partial p_{\mathrm{mD}}(z_{\mathrm{mD}}, t_{\mathrm{D}})}{\partial t_{\mathrm{D}}} = \lambda[p_{\mathrm{fD}}(r_{\mathrm{D}}, z_{\mathrm{D}}, t_{\mathrm{D}}) - p_{\mathrm{mD}}(z_{\mathrm{mD}}, t_{\mathrm{D}})] \tag{37}$$

Also, the $f(\mathrm{s})$ expression for transient matrix–fracture exchange (assuming a slab-shaped matrix block), Eq. (35), can be obtained by finding the relation between $\bar{p}_{\mathrm{fD}}(r_{\mathrm{D}}, z_{\mathrm{D}}, \mathrm{s})$ and $\bar{p}_{\mathrm{mD}}(z_{\mathrm{mD}}, \mathrm{s})$, Eq. (55), via Laplace solution of following governing equation, Eq. (38), accompanied with the appropriate initial condition, Eq. (24), and boundary conditions, Eqs. (39) and (40), for transient pressure variation inside the matrix block (Serra et al. 1983; Ozkan et al. 1987; Stewart and Asharsobbi 1988; Da Prat 1990; Sabet 1991; Al-Bemani and Ershaghi 1997; Hassanzadeh et al. 2009):

$$\frac{\partial^2 p_{\mathrm{mD}}(z_{\mathrm{mD}}, t_{\mathrm{D}})}{\partial z_{\mathrm{mD}}^2} = \frac{3(1-\omega)}{\lambda}\frac{\partial p_{\mathrm{mD}}(z_{\mathrm{mD}}, t_{\mathrm{D}})}{\partial t_{\mathrm{D}}} \tag{38}$$

$$\frac{\partial p_{\mathrm{mD}}(0, t_{\mathrm{D}})}{\partial z_{\mathrm{mD}}} = 0 \tag{39}$$

$$p_{\mathrm{mD}}(1, t_{\mathrm{D}}) = p_{\mathrm{fD}} \tag{40}$$

The Laplace inversion transforms in Eqs. (32) and (33) can be done by applying a numerically Laplace inversion method (Hassanzadeh and Pooladi-Darvish 2007; Mashayekhizadeh et al. 2011). In this work, the Stehfest (1970) method is applied for a numerical Laplace inversion.

In the following section, we present the results for the well response in an infinite-acting double-porosity reservoir with pseudo-steady-state and transient mass exchanges between the matrix and the fractures.

Table 1 The values of presented parameters in the developed model for the generation of Figs. 2, 3, 4 and 6, 7, 8

Parameter	Value
Dimensionless horizontal-to-vertical fracture permeability ratio, k_{fD}	10
Dimensionless total thickness of oil zone, h_{oD}	200
Dimensionless perforated thickness of oil zone, h_{pD}	40
Dimensionless perforation interval, h_D	0.2

3 Results

3.1 Pseudo-Steady-State Matrix–Fracture Exchange Formulation

The pseudo-steady state matrix–fracture exchange assumes that the rate of change of pressure in the matrix blocks is constant. One of the characteristics of a pseudo-steady exchange between the matrix and the fractures is a sharp dip in the derivative curve during the transition period.

In this section, the pseudo-steady state formulation has been used for the matrix–fracture exchange term, in order to study the effects of the interporosity flow coefficient, the storativity ratio, the skin factor, the wellbore storage coefficient and the penetration interval on the response of a partially penetrated well-producing from a 2D infinite-acting double-porosity reservoir with a gas cap.

3.1.1 Effects of the Interporosity Flow Coefficient and the Storativity Ratio

In this section, the effects of the interporosity flow coefficient and storativity ratio are studied. Table 1 shows the values of the parameters used in our analysis.

The interporosity flow coefficient determines the ability of the matrix to flow to the fractures and is a function of the matrix block size and permeability (Eq. 36). In a traditional double-porosity model, the interporosity flow coefficient governs the start time of the transition from the fracture system radial flow to the total (fracture and matrix) system radial flow and controls the speed at which the matrix reacts to the pressure depletion. Therefore, the interporosity flow coefficient dictates the duration of the transition (Houzé et al. 2007).

Figure 2a, b shows the effect of the interporosity flow coefficient on the dimensionless average pressure response of a partially penetrated well and its derivative versus dimensionless time for a 2D infinite-acting double-porosity reservoir, respectively. To develop these figures, we used Eqs. (30) and (31) and parameters given in Table 1, with $S = 0$, $C_{sD} = 0$ and $\omega = 0.01$. The interporosity flow coefficient values of 10^{-5}, 10^{-6}, 10^{-7} and 10^{-8} were used. Throughout this paper, the black curves in the figures demonstrate the response of a fully penetrated well versus dimensionless time obtained using $S = 0$, $C_{sD} = 0$, $\lambda = 10^{-6}$ and $\omega = 0.01$.

The results shown in Fig. 2a reveal that as the interporosity flow coefficient increases, the dimensionless average pressure response of the well decreases. However, eventually all of the dimensionless average pressure curves converge and are stabilized at a constant value, indicating a constant pressure support from the gas cap. The two parallel lines observed in the semi-log plot for radial double-porosity models without a gas cap are not evident in a double-porosity model with a gas cap. In other words, the traditional total system (matrix and fracture) radial flow response cannot be seen in the latter case, indicating that the gas cap effect is dominant.

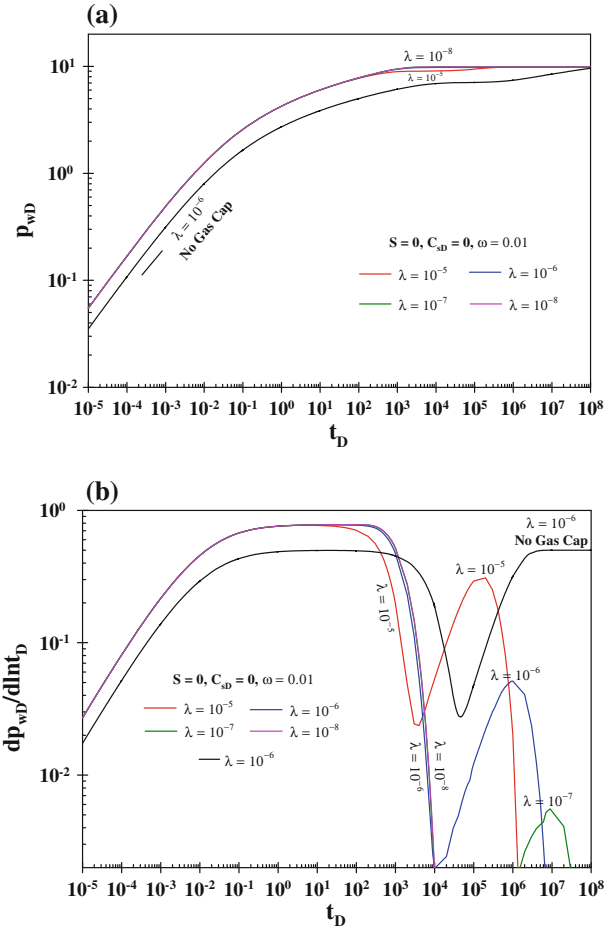

Fig. 2 Effect of different interporosity flow coefficients (λ) on **a** the dimensionless average pressure of a partially penetrated well (p_{wD}) and **b** its derivative ($dp_{wD}/d\ln t_D$) versus dimensionless time (t_D) for a 2D infinite-acting double-porosity reservoir with a gas cap. The *black curves* demonstrate the dimensionless average pressure of a fully penetrated well and its derivative versus dimensionless time for a radial infinite-acting double-porosity reservoir without a gas cap. In all of these calculations, a pseudo-steady-state formulation is assigned for the matrix–fracture exchange term. Data used in this figure are given in Table 1

The results shown in Fig. 2b reveal that the fracture dominated flow can be seen clearly for all interporosity flow coefficient values. As the interporosity flow coefficient increases, the fracture-dominated flow decreases. In other words, the matrix permeability is relatively high for a higher interporosity flow coefficient; therefore, it begins to respond to the pressure depletion in the fracture sooner. Moreover, for a high interporosity flow coefficient, the generated sharp dip is shallower. On the other hand, the matrix is very tight for a low interporosity flow coefficient, and the matrix begins to react to the pressure drop in the fracture later. Therefore, the fracture-dominated flow is sustained for a longer period.

As apparent in the average well pressure plot, the results in Fig. 2b demonstrate that for all values of the interporosity flow coefficient, the gas cap becomes dominant before the traditional total system radial flow is achieved. Therefore, the total system radial flow cannot

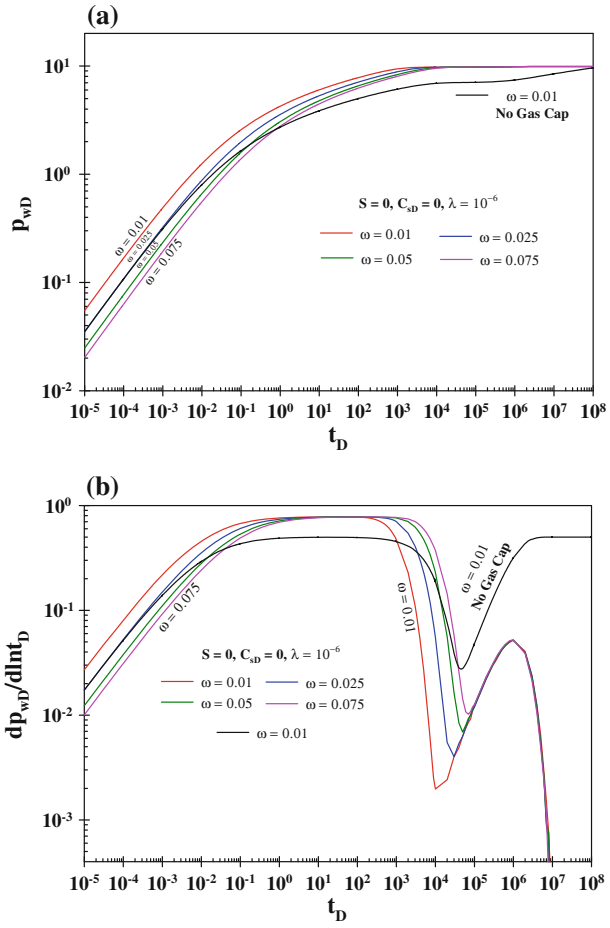

Fig. 3 Effect of different storativity ratios (ω) on **a** the dimensionless average pressure of a partially penetrated well (p_{wD}) and **b** its derivative ($dp_{\mathrm{wD}}/d\ln t_{\mathrm{D}}$) versus dimensionless time (t_{D}) for a 2D infinite-acting double-porosity reservoir with a gas cap. The *black curves* demonstrate the dimensionless average pressure response of a fully penetrated well and its derivative versus dimensionless time for a radial infinite-acting double-porosity reservoir without a gas cap. In all of these calculations, a pseudo-steady-state formulation is assigned for the matrix–fracture exchange term. Data used in this figure are given in Table 1

be seen for all interporosity flow coefficient values. Due to the predominant gas cap effect, the dimensionless average pressure response of the well is stabilized (Fig. 2a), and the derivative of the dimensionless average pressure response of the well goes to zero for large values of the dimensionless time (Fig. 2b). The results also demonstrate that the effect of the gas cap is more significant at lower interporosity flow coefficient values.

The storativity ratio specifies the fraction of the total interconnected pore volume occupied by the fractures (Eq. 14). In a traditional double-porosity model, the storativity ratio determines the depth of the generated dip during the transition from the fracture radial flow to the total system radial flow (Houzé et al. 2007). Figure 3a, b shows the effect of the storativity ratio on the dimensionless average pressure and its derivative versus dimensionless time, respectively. To develop these figures, we used Eqs. (30) and (31) and parameters given in

Table 1, with $S = 0$, $C_{sD} = 0$ and $\lambda = 10^{-6}$. Values of 0.01, 0.025, 0.05, and 0.075 were considered for the storativity ratio.

From Fig. 3a, it is possible to see that as the storativity ratio increases, the dimensionless average pressure of the well decreases. However, eventually all of the dimensionless average pressure curves are stabilized at a constant value.

The results shown in Fig. 3b reveal that the fracture flow can be clearly seen for all storativity ratio values. The effect of the storativity ratio on the onset time of transition flow is similar to that of the traditional double-porosity model without a gas cap, where a low storativity ratio demonstrates earlier commencement of the transition flow. The same observation can be made from the derivative plot, as shown in Fig. 3b. Another observation is that the gas cap effect creates a deeper v-shape in the derivative plot compared to that of a double-porosity model without a gas cap.

3.1.2 Effects of the Skin Factor and the Wellbore Storage- Coefficient

In this section, the effects of the skin factor and wellbore storage-coefficient are presented. Equations (30) and (31) were used to generate the dimensionless average pressure versus dimensionless time. Table 1 shows the values of the parameters used in our analysis. Figure 4a, b demonstrates the respective variations of the dimensionless average pressure and its derivative versus dimensionless time for different dimensionless wellbore storage- coefficients and skin factors. For the results shown in Fig. 4a, b, the interporosity flow coefficient and storativity ratio are considered to be 10^{-6} and 0.01, respectively. The values of 0, 10^2, 10^3, 10^4, and 10^5 are used for the dimensionless wellbore storage-coefficient, and the skin factor values are -5, 0, 5, 10, 15, and 20.

The results shown in Fig. 4a reveal that for a constant dimensionless wellbore storage-coefficient, as the skin factor increases, the dimensionless average pressure response of the well also increases. Moreover, for a constant skin factor, when the wellbore storage-coefficient increases, the stabilization time of the pressure also increases.

The wellbore storage effects appear as a unit slope line in the derivative plot shown in Fig. 4b. The results show that for small wellbore storage (i.e., $C_{sD} \leq 10^3$), a sharp dip during the transition period can be clearly observed for all skin factors. In addition, fracture flow can also be observed only when the skin factor is negative and the wellbore storage effect is low. However, at high values of wellbore storage and positive skin factor values, the v-shaped dip is not observed, due to the overriding effect of the gas cap. In all cases, the total system radial flow can be totally masked by the gas cap effect.

3.1.3 Effect of the Dimensionless Perforation Interval

In this section, the effect of perforation interval is studied. Table 2 shows the values of parameters used in our analysis. Figure 5a, b shows the effect of dimensionless perforation interval on the dimensionless average pressure response and its derivative versus dimensionless time, respectively. To develop Fig. 5a, b, we used Eqs. (30) and (31) along with parameters stated in Table 2 and $k_{fD} = 10$. The values of 0.2, 0.4, 0.6, 0.8, and 1 are chosen for dimensionless perforation interval.

Results shown in Fig. 5a reveal that as the dimensionless perforation interval decreases, the dimensionless average pressure response increases. The dimensionless average pressure response differs by a factor of $h_D = h_p/h_o$ (Eq. 22) as compared with the response of a fully penetrated well. Finally, each curve stabilizes at the late time at a constant value indicating a constant pressure support from the gas cap.

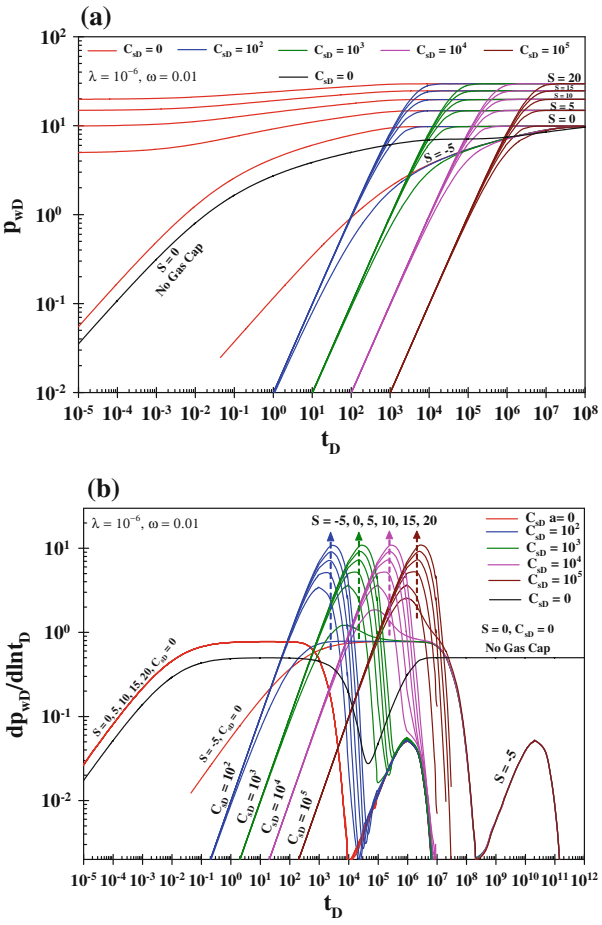

Fig. 4 Effect of different skin factors (S) and dimensionless wellbore storage coefficients (C_{sD}) on **a** the dimensionless average pressure response of a partially penetrated well (p_{wD}) and **b** its derivative ($dp_{wD}/dlnt_D$) versus dimensionless time (t_D) for an infinite-acting double-porosity reservoir with a gas cap. The *black curves* demonstrate the dimensionless average pressure response of a fully penetrated well and its derivative versus dimensionless time for an infinite-acting double-porosity reservoir without a gas cap. In all of these calculations, a pseudo-steady-state formulation is assigned for the matrix–fracture exchange term. Data used in this figure are given in Table 1

Table 2 The values of presented parameters in developed model for generation of Figs. 5 and 9

Parameter	Value
Skin factor, S (dimensionless)	0
Dimensionless wellbore storage coefficient, C_{sD}	0
Matrix–fracture interporosity flow coefficient, λ (dimensionless)	10^{-6}
Storativity ratio, ω (dimensionless)	0.01

According to Fig. 5b, the derivative of the dimensionless average pressure response also varies by a factor of $h_D = h_p/h_o$ (Eq. 22). Also Fig. 5b demonstrates that for all values of dimensionless perforation interval, the fracture system radial flow is observed clearly. As the dimensionless perforation interval increases, the fracture system radial flow becomes shorter. In other words, for a higher dimensionless perforation interval, the matrix begins to respond to the pressure depletion in the fracture sooner. Moreover, for a high dimensionless perforation interval, the generated sharp dip is deeper. On the other hand, for a small dimensionless perforation interval, the matrix begins to react to the pressure drop in the fracture later.

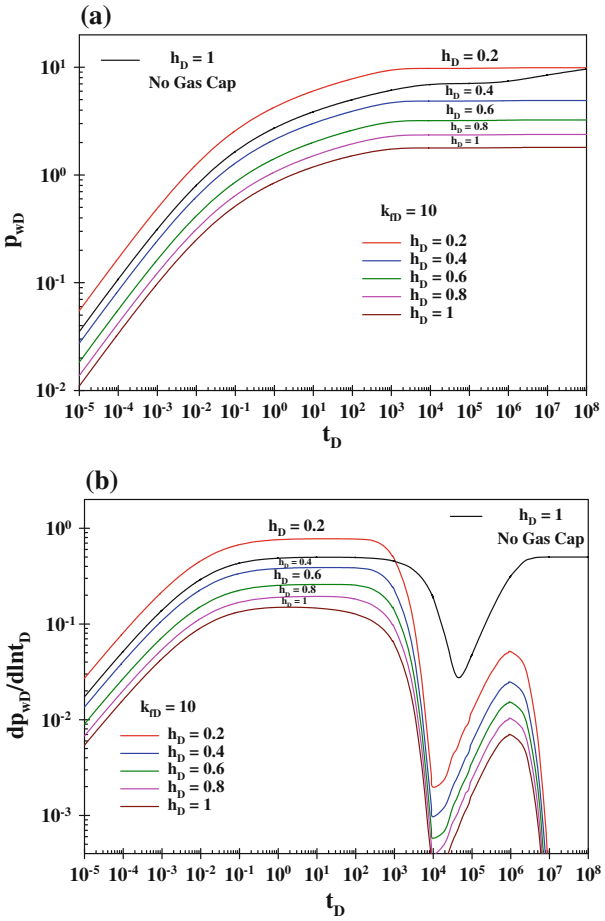

Fig. 5 Effect of different dimensionless perforation interval (h_D) on **a** the dimensionless average pressure (p_{wD}) and **b** its derivative ($dp_{wD}/d\ln t_D$) versus dimensionless time (t_D) for an infinite-acting double-porosity reservoir with a gas cap. The *black curves* demonstrate the dimensionless average pressure response of a fully penetrated well and its derivative versus dimensionless time for an infinite-acting double-porosity reservoir without a gas cap. In all of these calculations, a pseudo-steady-state formulation is assigned for the matrix–fracture exchange term. Data used in this figure are given in Table 2

Therefore, the fracture system radial flow sustains for a longer period. The time at which the derivative of the dimensionless average pressure is at minimum during the transition from fracture system radial flow to the total (fracture and matrix) system radial flow, is almost the same for all values of dimensionless perforation interval.

As it is apparent in the average well pressure plot, results in Fig. 5b demonstrate that for all values of dimensionless perforation interval, the gas cap begins to become dominant before the total system (fracture and matrix) radial flow is achieved. Therefore, the traditional half slope for the total system (fracture and matrix) radial flow cannot be observed for all values of dimensionless perforation interval. Due to prevailing gas cap effect, the dimensionless average pressure response of the well stabilizes (see Fig. 5a) and the derivative of the dimensionless average pressure goes to zero for large values of the dimensionless time (see Fig. 5b).

Results also demonstrate that the gas cap almost has the same effect for all values of dimensionless perforation interval.

3.2 Transient Matrix–Fracture Exchange Formulation

The transient matrix–fracture exchange model assumes that a pressure gradient exists within the matrix blocks. If the pressure distribution inside the matrix blocks is significant, the geometry of the matrix blocks has to be taken into consideration (Houzé et al. 2007). In this study, the matrix blocks are considered to be slab-shaped.

In this section, the transient formulation is used for the matrix–fracture exchange term to study the effects of the interporosity flow coefficient, storativity ratio, skin factor, wellbore storage-coefficient, and the penetration interval on the pressure response.

3.2.1 Effects of the Interporosity Flow Coefficient and the Storativity Ratio

In this section, the effects of the interporosity flow coefficient and the storativity ratio are presented. Table 1 shows the values of the parameters used in our analysis. Figure 6a, b shows the effects of the interporosity flow coefficient on the dimensionless average pressure and its derivative versus dimensionless time, respectively. To develop these figures, we used Eqs. (30) and (31) with $S = 0, C_{sD} = 0$ and $\omega = 0.01$. Values of 10^{-5}, 10^{-6}, 10^{-7}, and 10^{-8} were selected for the interporosity flow coefficient.

Figure 6a shows that as the interporosity flow coefficient increases, the dimensionless average pressure response of the well decreases. However, eventually all of the dimensionless average pressure curves converge to a constant value when the gas cap effect becomes dominant.

The results from Fig. 6b reveal that as the interporosity flow coefficient increases, the fracture flow period becomes shorter. For an interporosity flow coefficient of 10^{-5} (high matrix permeability), the fracture flow cannot be easily recognized. The results also show that the effect of gas cap becomes dominant during the transition flow before the traditional total fracture and matrix flow is achieved. Therefore, the combined fracture and matrix system flow cannot be seen for all interporosity flow coefficient values.

Figure 7a, b shows the effect of the storativity ratio on the dimensionless average pressure response and its derivative versus dimensionless time, respectively. To develop these figures, we applied Eqs. (30) and (31) and parameters given in Table 1, with $S = 0, C_{sD} = 0$ and $\lambda = 10^{-6}$. Values of 0.01, 0.025, 0.05, and 0.075 were used for the storativity ratio.

Figure 7a shows that as the storativity ratio increases, the dimensionless average pressure response of the well decreases. However, eventually all of the dimensionless average pressure curves are stabilized at a constant value when the gas cap becomes dominant. The results shown in Fig. 7b reveal that the fracture flow can be clearly seen for all storativity ratio values. For a low storativity ratio, the onset of the fracture flow starts and ends earlier.

Figure 7b shows that for a low storativity ratio, the matrix begins to react to the pressure drop earlier. Conversely, for a high storativity ratio, this response is delayed. As can be seen from Fig. 7b, for all storativity ratio values, the gas cap effect becomes dominant during the transition flow, and the traditional dip in the derivative plot cannot be observed.

3.2.2 Effects of the Skin Factor and the Wellbore Storage- Coefficient

In this section, the effects of the skin factor and wellbore storage-coefficient are presented. Equations (30) and (31) and the parameters in Table 1 were used to generate the dimensionless

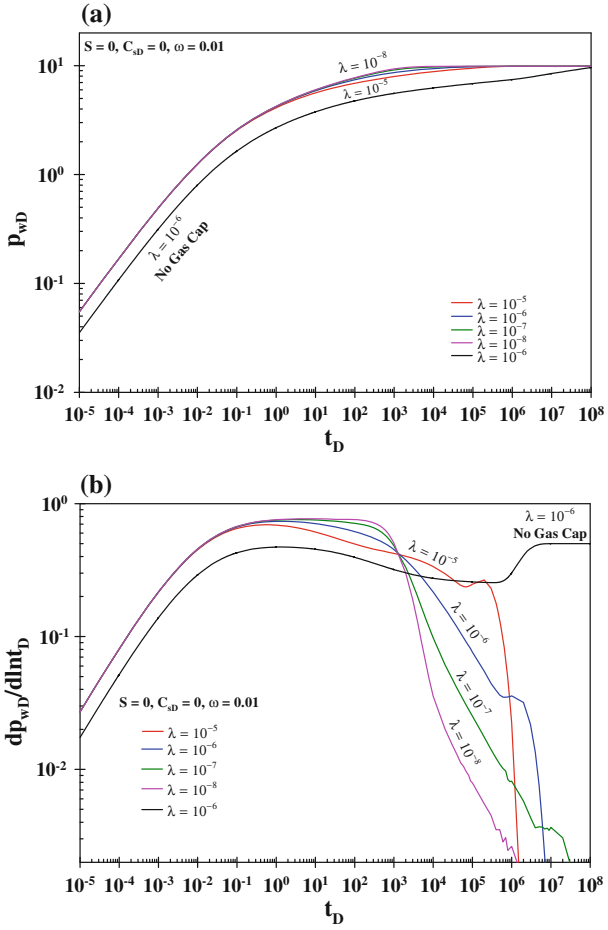

Fig. 6 Effect of different interporosity flow coefficients (λ) on **a** the dimensionless average pressure (p_{wD}) and **b** its derivative ($dp_{\mathrm{wD}}/d\ln t_{\mathrm{D}}$) versus dimensionless time (t_{D}) for a 2D infinite-acting double-porosity reservoir with a gas cap. The *black curves* demonstrate the dimensionless average pressure of a fully penetrated well and its derivative versus dimensionless time for a radial infinite-acting double-porosity reservoir without a gas cap. In all of these calculations, a transient formulation is assigned for the matrix–fracture exchange term. Data used in this figure are given in Table 1

average pressure response versus dimensionless time. Figure 8a, b demonstrates the respective variations of the dimensionless average pressure and the derivative of the dimensionless average pressure versus dimensionless time for different wellbore storage coefficients and skin factors. The interporosity flow coefficient and storativity ratio are considered to be 10^{-6} and 0.01, respectively. The values of the dimensionless wellbore storage coefficients are 0, 10^2, 10^3, 10^4, and 10^5, and the skin factor values are -5, 0, 5, 10, 15, and 20.

The results shown in Fig. 8a reveal that for a constant dimensionless wellbore storage-coefficient, as the skin factor increases, the dimensionless average pressure increases, revealing a larger pressure drop in the wellbore. The results also show that for a constant skin factor, the dimensionless time for stabilization increases when the dimensionless wellbore storage-coefficient increases.

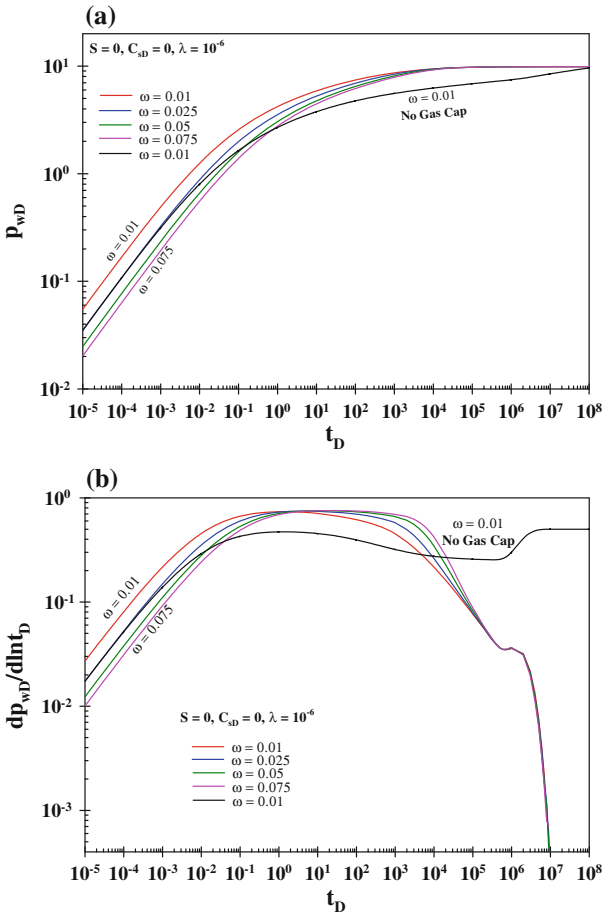

Fig. 7 Effect of different storativity ratios (ω) on **a** the dimensionless average pressure (p_{wD}) and **b** its derivative ($dp_{\mathrm{wD}}/d\ln t_{\mathrm{D}}$) versus dimensionless time (t_{D}) for a 2D infinite-acting double-porosity reservoir with a gas cap. The *black curves* demonstrate the dimensionless average pressure response of a fully penetrated well and its derivative versus dimensionless time for a radial infinite-acting double-porosity reservoir without a gas cap. In all of these calculations, a transient formulation is assigned for the matrix–fracture exchange term. Data used in this figure are given in Table 1

Figure 8b reveals that for a zero wellbore storage- coefficient and any skin factor value, the fracture flow can be clearly perceived. The results show that it may be possible to observe the dip in the derivative plot for a weak wellbore storage effect. However, it is not possible to detect such a dip when the wellbore storage effect is strong. In addition, the traditional combined matrix and fracture flow cannot be observed on the derivative plot. In other words, the gas cap effect becomes dominant early in the test so that the gas cap governs the overall behavior of the system.

3.2.3 Effect of the Dimensionless Perforation Interval

In this section, the effect of dimensionless perforation interval is studied. Table 2 shows the values of parameters used in our analysis. Figure 9a, b shows the effect of dimensionless

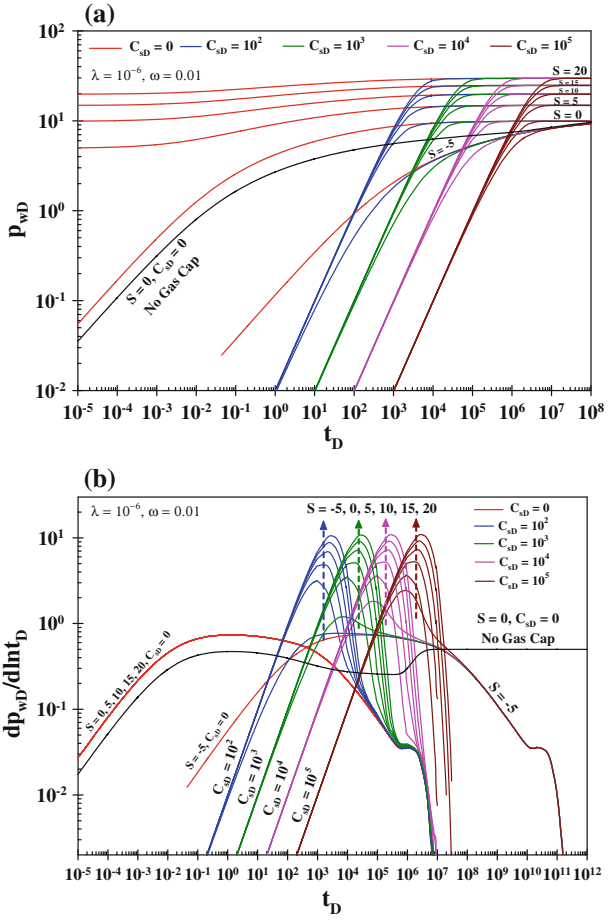

Fig. 8 Effect of different skin factors (S) and dimensionless wellbore storage-coefficients (C_{sD}) on **a** the dimensionless average pressure response (p_{wD}) and **b** its derivative ($dp_{wD}/d\ln t_D$) versus dimensionless time (t_D) for an infinite-acting double-porosity reservoir with a gas cap. The *black curves* demonstrate the dimensionless average pressure response of a fully penetrated well and its derivative versus dimensionless time for an infinite-acting double-porosity reservoir without a gas cap. In all of these calculations, a transient formulation is assigned for the matrix–fracture exchange term. Data used in this figure are given in Table 1

perforation interval on the dimensionless average pressure response, respectively. To develop Fig. 9a, b, we used Eqs. (30) and (31) along with parameters stated in Table 2 and $k_{fD} = 10$. The values of 0.2, 0.4, 0.6, 0.8, and 1 are chosen for dimensionless perforation interval.

Results shown in Fig. 9a reveal that as the dimensionless perforation interval decreases, the dimensionless average pressure response increases. The dimensionless average pressure response of the well differs by a factor of $h_D = h_p/h_o$ (Eq. 22). Eventually, each curve stabilizes at the late time at a constant value indicating a constant pressure support from the gas cap.

According to Fig. 9b, the derivative of the dimensionless average pressure response of the well varies by a factor of $h_D = h_p/h_o$ (Eq. 22). Also Fig. 9b shows that for all values of dimensionless perforation interval, the fracture system radial flow is seen clearly. As the dimensionless perforation interval increases, the fracture system radial flow becomes shorter.

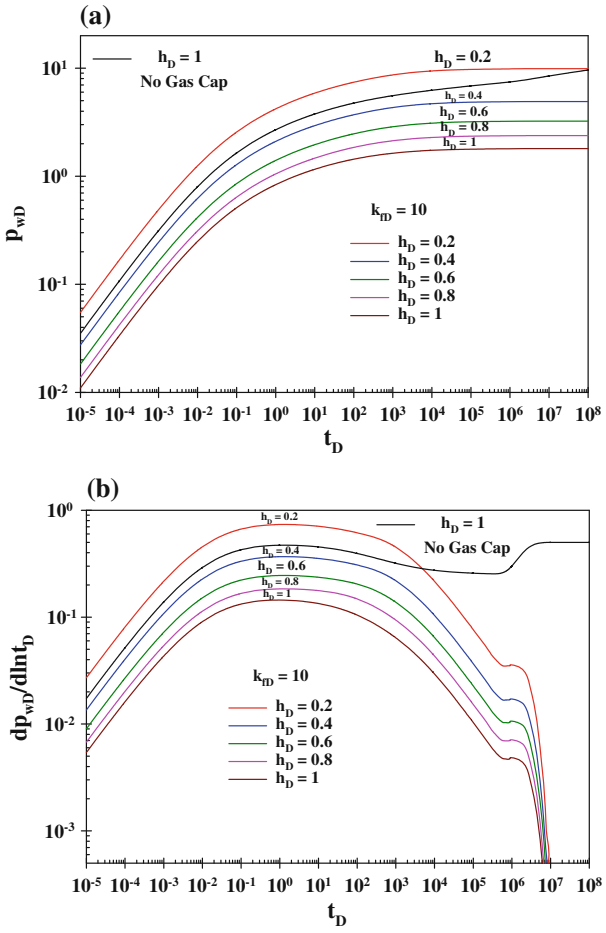

Fig. 9 Effect of different dimensionless perforation interval (h_D) on **a** the dimensionless average pressure response (p_{wD}) and **b** its derivative ($dp_{wD}/d\ln t_D$) versus dimensionless time (t_D) for an infinite-acting double-porosity reservoir with a gas cap. The *black curves* demonstrate the dimensionless average pressure response of a fully penetrated well and its derivative versus dimensionless time for an infinite-acting double-porosity reservoir without a gas cap. In all of these calculations, a transient formulation is assigned for the matrix–fracture exchange term. Data used in this figure are given in Table 2

In other words, for a higher dimensionless perforation interval, the matrix begins to respond to the pressure depletion in the fracture sooner. For all values of dimensionless perforation interval, the right-hand half of the dip cannot be formed due to the gas cap effect. Moreover, for a small dimensionless perforation interval, the matrix begins to react to the pressure drop in the fracture later. Therefore, the fracture system radial flow sustains for a longer period.

The time at which the derivative of the dimensionless average pressure response is at minimum during the transition period (the bottom of the generated dip), is the same for all values of dimensionless perforation interval.

As it was apparent in the average well pressure plot, results in Fig. 9b demonstrate that for all values of dimensionless perforation interval, the gas cap begins to become dominant before the right-hand half of the dip is achieved. Due to prevailing gas cap effect, the dimensionless average pressure stabilizes (see Fig. 9a) and the derivative of the dimensionless average

pressure response of the well goes to zero for large values of the dimensionless time (see Fig. 9b). Results also demonstrate that the gas cap almost has the same effect for all values of perforation interval.

4 Summary and Conclusions

In this paper, we have studied the pressure transient behavior of a partially penetrated well in an infinite-acting double-porosity system with a constant pressure at the top boundary, based on a semi-analytical solution of the 2D diffusivity equation using successive Laplace and modified finite Fourier sine transforms. We have considered both pseudo-steady-state and transient formulations for the matrix–fracture exchange term in this 2D double-porosity model. These analytical solutions can be used to generate type curves for the pressure transient analysis of wellbores in naturally fractured oil reservoirs with a gas cap.

Sensitivity analyses have been presented for both pseudo-steady- state and transient matrix–fracture exchanges to investigate the effects of the interporosity flow coefficient, the storativity ratio, the wellbore storage coefficient, the skin factor, and the perforation interval. The results show that in the presence of wellbore storage, the early period fracture flow can be easily masked and the wellbore storage effect appears as a unit slope line in the derivative plot. The late-period combined matrix and fracture flow is not evident, due to the gas cap effect. Therefore, the two parallel lines observed in the traditional semi-log plot for radial double-porosity models without a gas cap are not apparent in a double-porosity model with a gas cap, and a conventional semi-log analysis is not possible. In addition, it has been shown that it is possible to observe the v-dip in the derivative plot for a weak wellbore storage effect; however, it is not possible to see such a dip when the wellbore storage effect is strong.

Acknowledgements The authors would like to thank Dr. Ali M. Saidi for his encouragement and insights. The first author is appreciative of the support of his parents, Dariush Dejam and Zahra Fakhari. They have been a source of encouragement and inspiration. Financial support of NSERC/AERI/Foundation CMG and iCORE Chairs Funds is gratefully acknowledged.

Appendix: Derivation of Solutions

The details of the derivations for obtaining the dimensionless average pressure response of a partially penetrated well in the oil zone of an infinite-acting double-porosity reservoir including wellbore storage and skin effects are presented in this appendix.

First, we define the Laplace transforms with respect to t_D for dimensionless fracture and matrix pressures, respectively, as follows:

$$\bar{p}_{fD}(r_D, z_D, s) = \ell_{t_D}\{p_{fD}(r_D, z_D, t_D)\} = \int_0^{+\infty} e^{-st_D} p_{fD}(r_D, z_D, t_D) dt_D \tag{41}$$

$$\bar{p}_{mD}(z_{mD}, s) = \ell_{t_D}\{p_{mD}(z_{mD}, t_D)\} = \int_0^{+\infty} e^{-st_D} p_{mD}(z_{mD}, t_D) dt_D \tag{42}$$

where $\bar{p}_{fD}$ and $\bar{p}_{mD}$ are the dimensionless fracture and matrix pressures in the Laplace domain, respectively; "s" is the variable of the Laplace transform; ℓ_{t_D} is the sign for the Laplace transform with respect to t_D.

After applying the Laplace transform with respect to t_D for the boundary conditions in Eqs. (25–29), we have:

$$\left(\frac{\partial \bar{p}_{fD}(r_D, z_D, s)}{\partial r_D}\right)_{r_D=r_{wD}} = 0 \quad 0 < z_D < h_{oD} - h_{pD} \tag{43}$$

$$\begin{cases} \bar{p}_{fD,S}(r_{wD}, z_D, s) = \left[\bar{p}_{fD}(r_D, z_D, s) - h_D\left(\frac{\partial \bar{p}_{fD}(r_D, z_D, s)}{\partial r_D}\right) S\right]_{r_D=r_{wD}} \\ sC_{sD}\bar{p}_{fD,S}(r_{wD}, z_D, s) - h_D\left(\frac{\partial \bar{p}_{fD}(r_D, z_D, s)}{\partial r_D}\right)_{r_D=r_{wD}} = \frac{1}{s} \end{cases} \quad h_{oD} - h_{pD} < z_D < h_{oD} \tag{44}$$

$$\bar{p}_{fD}(+\infty, z_D, s) = 0 \tag{45}$$

$$\bar{p}_{fD}(r_D, 0, s) = 0 \tag{46}$$

$$\frac{\partial \bar{p}_{fD}(r_D, h_{oD}, s)}{\partial z_D} = 0 \tag{47}$$

Applying the Laplace transform with respect to t_D to Eq. (23) results in:

$$\frac{\partial^2 \bar{p}_{fD}(r_D, z_D, s)}{\partial r_D^2} + \frac{1}{r_D}\frac{\partial \bar{p}_{fD}(r_D, z_D, s)}{\partial r_D} + \frac{\partial^2 \bar{p}_{fD}(r_D, z_D, s)}{\partial z_D^2} = k_{fD}\left[\omega \ell_{t_D}\left\{\frac{\partial p_{fD}(r_D, z_D, t_D)}{\partial t_D}\right\} + (1-\omega)\ell_{t_D}\left\{\frac{\partial p_{mD}(z_{mD}, t_D)}{\partial t_D}\right\}\right] \tag{48}$$

Where

$$\ell_{t_D}\left\{\frac{\partial p_{fD}(r_D, z_D, t_D)}{\partial t_D}\right\} = s\bar{p}_{fD}(r_D, z_D, s) - p_{fD}(r_D, z_D, 0) \tag{49}$$

And

$$\ell_{t_D}\left\{\frac{\partial p_{mD}(z_{mD}, t_D)}{\partial t_D}\right\} = s\bar{p}_{mD}(z_{mD}, s) - p_{mD}(z_{mD}, 0) \tag{50}$$

Using Eqs. (24) and (49), Eq. (50) reduces to:

$$\ell_{t_D}\left\{\frac{\partial p_{fD}(r_D, z_D, t_D)}{\partial t_D}\right\} = s\bar{p}_{fD}(r_D, z_D, s) \tag{51}$$

And

$$\ell_{t_D}\left\{\frac{\partial p_{mD}(z_{mD}, t_D)}{\partial t_D}\right\} = s\bar{p}_{mD}(z_{mD}, s) \tag{52}$$

Combining Eqs. (48), (51) and (52), we obtain:

$$\frac{\partial^2 \bar{p}_{fD}(r_D, z_D, s)}{\partial r_D^2} + \frac{1}{r_D}\frac{\partial \bar{p}_{fD}(r_D, z_D, s)}{\partial r_D} + \frac{\partial^2 \bar{p}_{fD}(r_D, z_D, s)}{\partial z_D^2} = k_{fD}[\omega_s \bar{p}_{fD}(r_D, z_D, s) + (1-\omega)s\bar{p}_{mD}(z_{mD}, s)] \tag{53}$$

The following relation between $\bar{p}_{fD}$ and $\bar{p}_{mD}$ can be obtained for the pseudo-steady-state matrix–fracture exchange (Warren and Root 1963):

$$\bar{p}_{mD}(z_{mD}, s) = \frac{\lambda}{\lambda + (1-\omega)s}\bar{p}_{fD}(r_D, z_D, s) \tag{54}$$

Also, the following relation between $\bar{p}_{\mathrm{fD}}$ and $\bar{p}_{\mathrm{mD}}$ can be obtained for the transient matrix–fracture exchange (Serra et al. 1983; Ozkan et al. 1987; Stewart and Asharsobbi 1988; Da Prat 1990; Sabet 1991; Al-Bemani and Ershaghi 1997; Hassanzadeh et al. 2009):

$$\bar{p}_{\mathrm{mD}}(z_{\mathrm{mD}}, \mathrm{s}) = \frac{\tanh\left(\sqrt{\frac{3(1-\omega)\mathrm{s}}{\lambda}}\right)}{\sqrt{\frac{3(1-\omega)\mathrm{s}}{\lambda}}} \bar{p}_{\mathrm{fD}}(r_{\mathrm{D}}, z_{\mathrm{D}}, \mathrm{s}) \tag{55}$$

By inserting Eqs. (54) and (55) into Eq. (53), it is possible to arrive at:

$$\frac{\partial^2 \bar{p}_{\mathrm{fD}}(r_{\mathrm{D}}, z_{\mathrm{D}}, \mathrm{s})}{\partial r_{\mathrm{D}}^2} + \frac{1}{r_{\mathrm{D}}} \frac{\partial \bar{p}_{\mathrm{fD}}(r_{\mathrm{D}}, z_{\mathrm{D}}, \mathrm{s})}{\partial r_{\mathrm{D}}} + \frac{\partial^2 \bar{p}_{\mathrm{fD}}(r_{\mathrm{D}}, z_{\mathrm{D}}, \mathrm{s})}{\partial z_{\mathrm{D}}^2} = k_{\mathrm{fD}} \mathrm{s} f(\mathrm{s}) \bar{p}_{\mathrm{fD}}(r_{\mathrm{D}}, z_{\mathrm{D}}, \mathrm{s}) \tag{56}$$

where $f(\mathrm{s})$ for the pseudo-steady-state matrix–fracture exchange is presented by (Warren and Root 1963):

$$f(s) = \omega + \frac{(1-\omega)\lambda}{\lambda + (1-\omega)s} \tag{57}$$

and $f(\mathrm{s})$ for the transient matrix–fracture exchange, assuming a slab-shaped matrix block, is given by (Serra et al. 1983; Ozkan et al. 1987; Stewart and Asharsobbi 1988; Da Prat 1990; Sabet 1991; Al-Bemani and Ershaghi 1997; Hassanzadeh et al. 2009):

$$f(\mathrm{s}) = \omega + \sqrt{\frac{\lambda(1-\omega)}{3\mathrm{s}}} \tanh\left(\sqrt{\frac{3(1-\omega)\mathrm{s}}{\lambda}}\right) \tag{58}$$

where λ is the matrix–fracture interporosity flow coefficient, defined as (Warren and Root 1963):

$$\lambda = \sigma \frac{r_{\mathrm{w}}^2 k_{\mathrm{m}}}{k_{\mathrm{fh}}} \tag{59}$$

where σ is the matrix–fracture transfer coefficient or the so-called shape factor, and k_{m} is the matrix permeability.

The modified finite Fourier sine transform with respect to z_{D} is defined for the dimensionless fracture pressure as follows:

$$\tilde{\bar{p}}_{\mathrm{fD}}(r_{\mathrm{D}}, n, \mathrm{s}) = \wp_{z_{\mathrm{D}}}\{\bar{p}_{\mathrm{fD}}(r_{\mathrm{D}}, z_{\mathrm{D}}, \mathrm{s})\} = \int_0^{h_{\mathrm{oD}}} \bar{p}_{\mathrm{fD}}(r_{\mathrm{D}}, z_{\mathrm{D}}, \mathrm{s}) \sin(a_n z_{\mathrm{D}}) dz_{\mathrm{D}} \tag{60}$$

where $\tilde{\bar{p}}_{\mathrm{fD}}$ is the modified finite Fourier sine transform of $\bar{p}_{\mathrm{fD}}$, n is the variable of the modified finite Fourier sine transform, $\wp_{z_{\mathrm{D}}}$ is the sign for the modified finite Fourier sine transform with respect to z_{D}, and a_n is a function of the variable of the modified finite Fourier sine transform, defined as:

$$a_n = \left(n - \frac{1}{2}\right)\frac{\pi}{h_{\mathrm{oD}}}, \qquad n = 1, 2, 3, \ldots \tag{61}$$

By applying the modified finite Fourier sine transform with respect to z_{D} for the inner and outer boundary conditions (44) and (45), which are defined in the Laplace domain,we have:

$$\int_0^{h_{oD}} \bar{p}_{fD,S}(r_{wD}, z_D, s)\sin(a_n z_D)dz_D = \left[\int_0^{h_{oD}} [\bar{p}_{fD}(r_D, z_D, s)]_{r_D=r_{wD}}\sin(a_n z_D)dz_D\right]$$
$$-h_D\left[\int_0^{h_{oD}}\left(\frac{\partial \bar{p}_{fD}(r_D, z_D, s)}{\partial r_D}\right)_{r_D=r_{wD}}\sin(a_n z_D)dz_D\right]S \quad (62)$$

$$sC_{sD}\left[\int_0^{h_{oD}} \bar{p}_{fD,S}(r_{wD}, z_D, s)\sin(a_n z_D)dz_D\right]$$
$$-h_D\left[\int_0^{h_{oD}}\left(\frac{\partial \bar{p}_{fD}(r_D, z_D, s)}{\partial r_D}\right)_{r_D=r_{wD}}\sin(a_n z_D)dz_D\right] = \left[\int_0^{h_{oD}}\frac{1}{s}\sin(a_n z_D)dz_D\right] \quad (63)$$

$$\int_0^{h_{oD}} \bar{p}_{fD}(+\infty, z_D, s)\sin(a_n z_D)dz_D = \tilde{\bar{p}}_{fD}(+\infty, n, s) = 0 \quad (64)$$

The integrals within interval $0 < z_D < h_{oD}$, which includes $[\partial \bar{p}_{fD}(r_D, z_D, s)/\partial r_D]_{r_D=r_{wD}}$, in Eqs. (62) and (63) are partitioned into two integrals for non-perforated interval, $0 < z_D < h_{oD} - h_{pD}$, and perforated interval, $h_{oD} - h_{pD} < z_D < h_{oD}$, as follows:

$$\tilde{\bar{p}}_{fD,S}(r_{wD}, n, s) = [\tilde{\bar{p}}_{fD}(r_D, n, s)]_{r_D=r_{wD}}$$
$$-h_D\left[\int_0^{h_{oD}-h_{pD}}\left(\frac{\partial \bar{p}_{fD}(r_D, z_D, s)}{\partial r_D}\right)_{r_D=r_{wD}}\sin(a_n z_D)dz_D\right.$$
$$\left.+\int_{h_{oD}-h_{pD}}^{h_{oD}}\left(\frac{\partial \bar{p}_{fD}(r_D, z_D, s)}{\partial r_D}\right)_{r_D=r_{wD}}\sin(a_n z_D)dz_D\right]S \quad (65)$$

$$sC_{sD}\tilde{\bar{p}}_{fD,S}(r_{wD}, n, s)$$
$$-h_D\left[\int_0^{h_{oD}-h_{pD}}\left(\frac{\partial \bar{p}_{fD}(r_D, z_D, s)}{\partial r_D}\right)_{r_D=r_{wD}}\sin(a_n z_D)dz_D\right.$$
$$\left.+\int_{h_{oD}-h_{pD}}^{h_{oD}}\left(\frac{\partial \bar{p}_{fD}(r_D, z_D, s)}{\partial r_D}\right)_{r_D=r_{wD}}\sin(a_n z_D)dz_D\right] = \frac{1}{sa_n} \quad (66)$$

Combination of Eqs. (43), (65) and (66) results in:

$$\tilde{\bar{p}}_{fD,S}(r_{wD}, n, s) = [\tilde{\bar{p}}_{fD}(r_D, n, s)]_{r_D=r_{wD}}$$
$$-h_D\left[\int_0^{h_{oD}-h_{pD}}(0)\sin(a_n z_D)dz_D + \int_{h_{oD}-h_{pD}}^{h_{oD}}\left(\frac{\partial \bar{p}_{fD}(r_D, z_D, s)}{\partial r_D}\right)_{r_D=r_{wD}}\sin(a_n z_D)dz_D\right]S \quad (67)$$

$$sC_{sD}\tilde{\bar{p}}_{fD,S}(r_{wD},n,s)-h_D\left[\int_0^{h_{oD}-h_{pD}}(0)\sin(a_nz_D)dz_D+\int_{h_{oD}-h_{pD}}^{h_{oD}}\left(\frac{\partial\bar{p}_{fD}(r_D,z_D,s)}{\partial r_D}\right)_{r_D=r_{wD}}\sin(a_nz_D)dz_D\right]=\frac{1}{sa_n} \tag{68}$$

By simplifying Eqs. (67) and (68), it is possible to arrive at:

$$\tilde{\bar{p}}_{fD,S}(r_{wD},n,s)=[\tilde{\bar{p}}_{fD}(r_D,n,s)]_{r_D=r_{wD}}-h_D\left[\int_{h_{oD}-h_{pD}}^{h_{oD}}\left(\frac{\partial\bar{p}_{fD}(r_D,z_D,s)}{\partial r_D}\right)_{r_D=r_{wD}}\sin(a_nz_D)dz_D\right]S \tag{69}$$

$$sC_{sD}\tilde{\bar{p}}_{fD,S}(r_{wD},n,s)-h_D\left[\int_{h_{oD}-h_{pD}}^{h_{oD}}\left(\frac{\partial\bar{p}_{fD}(r_D,z_D,s)}{\partial r_D}\right)_{r_D=r_{wD}}\sin(a_nz_D)dz_D\right]=\frac{1}{s,a_n} \tag{70}$$

In order to compute the integrals in Eqs. (69) and (70), it is necessary to differentiate with respect to r_D from both sides of Eq. (60) as follows:

$$\frac{\partial\tilde{\bar{p}}_{fD}(r_D,n,s)}{\partial r_D}=\int_0^{h_{oD}}\left(\frac{\partial\bar{p}_{fD}(r_D,z_D,s)}{\partial r_D}\right)\sin(a_nz_D)dz_D \tag{71}$$

It is possible to write Eq. (31) at $r_D=r_{wD}$:

$$\left(\frac{\partial\tilde{\bar{p}}_{fD}(r_D,n,s)}{\partial r_D}\right)_{r_D=r_{wD}}=\int_0^{h_{oD}}\left(\frac{\partial\bar{p}_{fD}(r_D,z_D,s)}{\partial r_D}\right)_{r_D=r_{wD}}\sin(a_nz_D)dz_D \tag{72}$$

The integral within interval $0<z_D<h_{oD}$ in right hand side of Eq. (72) is partitioned into two different integrals for non-perforated interval, $0<z_D<h_{oD}-h_{pD}$, and perforated interval, $h_{oD}-h_{pD}<z_D<h_{oD}$, as following:

$$\left(\frac{\partial\tilde{\bar{p}}_{fD}(r_D,n,s)}{\partial r_D}\right)_{r_D=r_{wD}}=\int_0^{h_{oD}-h_{pD}}\left(\frac{\partial\bar{p}_{fD}(r_D,z_D,s)}{\partial r_D}\right)_{r_D=r_{wD}}\sin(a_nz_D)dz_D+\int_{h_{oD}-h_{pD}}^{h_{oD}}\left(\frac{\partial\bar{p}_{fD}(r_D,z_D,s)}{\partial r_D}\right)_{r_D=r_{wD}}\sin(a_nz_D)dz_D \tag{73}$$

Combination of Eqs. (43) and (73) leads to:

$$\left(\frac{\partial \tilde{\bar{p}}_{\mathrm{fD}}(r_{\mathrm{D}},n,\mathrm{s})}{\partial r_{\mathrm{D}}}\right)_{r_{\mathrm{D}}=r_{\mathrm{wD}}} = \int_{0}^{h_{\mathrm{oD}}-h_{\mathrm{pD}}} (0)\sin(a_n z_{\mathrm{D}})dz_{\mathrm{D}} + \int_{h_{\mathrm{oD}}-h_{\mathrm{pD}}}^{h_{\mathrm{oD}}} \left(\frac{\partial \bar{p}_{\mathrm{fD}}(r_{\mathrm{D}},z_{\mathrm{D}},\mathrm{s})}{\partial r_{\mathrm{D}}}\right)_{r_{\mathrm{D}}=r_{\mathrm{wD}}} \sin(a_n z_{\mathrm{D}})dz_{\mathrm{D}} \tag{74}$$

After simplification, Eq. (74) turns to:

$$\left(\frac{\partial \tilde{\bar{p}}_{\mathrm{fD}}(r_{\mathrm{D}},n,\mathrm{s})}{\partial r_{\mathrm{D}}}\right)_{r_{\mathrm{D}}=r_{\mathrm{wD}}} = \int_{h_{\mathrm{oD}}-h_{\mathrm{pD}}}^{h_{\mathrm{oD}}} \left(\frac{\partial \bar{p}_{\mathrm{fD}}(r_{\mathrm{D}},z_{\mathrm{D}},\mathrm{s})}{\partial r_{\mathrm{D}}}\right)_{r_{\mathrm{D}}=r_{\mathrm{wD}}} \sin(a_n z_{\mathrm{D}})dz_{\mathrm{D}} \tag{75}$$

Combination of Eqs. (69), (70) and (75) results in:

$$\tilde{\bar{p}}_{\mathrm{fD,S}}(r_{\mathrm{wD}},n,\mathrm{s}) = \left[\tilde{\bar{p}}_{\mathrm{fD}}(r_{\mathrm{D}},n,\mathrm{s}) - h_{\mathrm{D}}\left(\frac{\partial \tilde{\bar{p}}_{\mathrm{fD}}(r_{\mathrm{D}},n,\mathrm{s})}{\partial r_{\mathrm{D}}}\right)S\right]_{r_{\mathrm{D}}=r_{\mathrm{wD}}} \tag{76}$$

$$sC_{\mathrm{sD}}\tilde{\bar{p}}_{\mathrm{fD,S}}(r_{\mathrm{wD}},n,s) - h_{\mathrm{D}}\left(\frac{\partial \tilde{\bar{p}}_{\mathrm{fD}}(r_{\mathrm{D}},n,\mathrm{s})}{\partial r_{\mathrm{D}}}\right)_{r_{\mathrm{D}}=r_{\mathrm{wD}}} = \frac{1}{\mathrm{s}a_n} \tag{77}$$

Applying the modified finite Fourier sine transform with respect to z_{D} to Eq. (56), which is defined in the Laplace domain, results in:

$$\frac{\partial^2 \tilde{\bar{p}}_{\mathrm{fD}}(r_{\mathrm{D}},n,\mathrm{s})}{\partial r_{\mathrm{D}}^2} + \frac{1}{r_{\mathrm{D}}}\frac{\partial \tilde{\bar{p}}_{\mathrm{fD}}(r_{\mathrm{D}},n,s)}{\partial r_{\mathrm{D}}} + \wp_{z_{\mathrm{D}}}\left\{\frac{\partial^2 \bar{p}_{\mathrm{fD}}(r_{\mathrm{D}},n,\mathrm{s})}{\partial z_{\mathrm{D}}^2}\right\} = k_{\mathrm{fD}}\mathrm{s}f(\mathrm{s})\tilde{\bar{p}}_{\mathrm{fD}}(r_{\mathrm{D}},n,\mathrm{s}) \tag{78}$$

where

$$\wp_{z_{\mathrm{D}}}\left\{\frac{\partial^2 \bar{p}_{\mathrm{fD}}(r_{\mathrm{D}},z_{\mathrm{D}},\mathrm{s})}{\partial z_{\mathrm{D}}^2}\right\} = -a_n^2\tilde{\bar{p}}_{\mathrm{fD}}(r_{\mathrm{D}},n,\mathrm{s}) + a_n\bar{p}_{\mathrm{fD}}(r_{\mathrm{D}},0,\mathrm{s}) - (-1)^n\frac{\partial \bar{p}_{\mathrm{fD}}(r_{\mathrm{D}},h_{\mathrm{oD}},\mathrm{s})}{\partial z_{\mathrm{D}}} \tag{79}$$

By applying the boundary conditions at the top ($z_{\mathrm{D}}=0$) and bottom ($z_{\mathrm{D}}=h_{\mathrm{oD}}$) of the oil zone of an infinite-acting fractured reservoir in the Laplace domain, i.e., Eqs. (46) and (47), it is possible to simplify Eq. (79) to:

$$\wp_{z_{\mathrm{D}}}\left\{\frac{\partial^2 \bar{p}_{\mathrm{fD}}(r_{\mathrm{D}},z_{\mathrm{D}},\mathrm{s})}{\partial z_{\mathrm{D}}^2}\right\} = -a_n^2\tilde{\bar{p}}_{\mathrm{fD}}(r_{\mathrm{D}},n,\mathrm{s}) \tag{80}$$

After inserting Eq. (80) into Eq. (79) and replacing ∂ by d, we arrive at:

$$\frac{d^2 \tilde{\bar{p}}_{\mathrm{fD}}(r_{\mathrm{D}},n,\mathrm{s})}{dr_{\mathrm{D}}^2} + \frac{1}{r_{\mathrm{D}}}\frac{d\tilde{\bar{p}}_{\mathrm{fD}}(r_{\mathrm{D}},n,\mathrm{s})}{dr_{\mathrm{D}}} - a_{\mathrm{n}}^2\tilde{\bar{p}}_{\mathrm{fD}}(r_{\mathrm{D}},n,\mathrm{s}) = k_{\mathrm{fD}}\mathrm{s}f(\mathrm{s})\tilde{\bar{p}}_{\mathrm{fD}}(r_{\mathrm{D}},n,\mathrm{s}) \tag{81}$$

With some rearrangements, Eq. (81) becomes:

$$\frac{d^2\tilde{\bar{p}}_{\mathrm{fD}}(r_{\mathrm{D}},n,\mathrm{s})}{dr_{\mathrm{D}}^2}+\frac{1}{r_{\mathrm{D}}}\frac{d\tilde{\bar{p}}_{\mathrm{fD}}(r_{\mathrm{D}},n,\mathrm{s})}{dr_{\mathrm{D}}}-\left[a_n^2+k_{\mathrm{fD}}sf(s)\right]\tilde{\bar{p}}_{\mathrm{fD}}(r_{\mathrm{D}},n,\mathrm{s})=0 \tag{82}$$

The square root of the expression inside the bracket in Eq. (82) is defined by η, as given by:

$$\eta=\sqrt{a_n^2+k_{\mathrm{fD}}\mathrm{s}f(\mathrm{s})} \tag{83}$$

Combining Eqs. (82) and (83) results in:

$$\frac{d^2\tilde{\bar{p}}_{\mathrm{fD}}(r_{\mathrm{D}},n,\mathrm{s})}{dr_{\mathrm{D}}^2}+\frac{1}{r_{\mathrm{D}}}\frac{d\tilde{\bar{p}}_{\mathrm{fD}}(r_{\mathrm{D}},n,\mathrm{s})}{dr_{\mathrm{D}}}-\eta^2\tilde{\bar{p}}_{\mathrm{fD}}(r_{\mathrm{D}},n,\mathrm{s})=0 \tag{84}$$

Equation (84) is a modified homogeneous Bessel differential equation that has the following general solution:

$$\tilde{\bar{p}}_{\mathrm{fD}}(r_{\mathrm{D}},n,\mathrm{s})=A_1I_0(\eta r_{\mathrm{D}})+A_2K_0(\eta r_{\mathrm{D}}) \tag{85}$$

where A_1 and A_2 are the first and second constants of the general solution (85), and I_0 and K_0 are the modified Bessel functions of the first and second kinds of order 0.

By applying Eq. (64) to Eq. (85), we can conclude that $A_1=0$; therefore, Eq. (85) reduces to:

$$\tilde{\bar{p}}_{\mathrm{fD}}(r_{\mathrm{D}},n,\mathrm{s})=A_2K_0(\eta r_{\mathrm{D}}) \tag{86}$$

By differentiation with respect to r_{D} from Eq. (86), we obtain:

$$\frac{\partial\tilde{\bar{p}}_{\mathrm{fD}}(r_{\mathrm{D}},n,\mathrm{s})}{\partial r_{\mathrm{D}}}=-A_2\eta K_1(\eta r_{\mathrm{D}}) \tag{87}$$

where K_1 is the modified Bessel function of the second kind of order 1.

By combining Eqs. (76), (86) and (87), it is possible to arrive at:

$$\tilde{\bar{p}}_{\mathrm{fD,S}}(r_{\mathrm{wD}},n,\mathrm{s})=A_2K_0(\eta r_{\mathrm{wD}})+Sh_{\mathrm{D}}A_2\eta K_1(\eta r_{\mathrm{wD}}) \tag{88}$$

By combining Eqs. (77), (86) and (87), we have:

$$sC_{\mathrm{sD}}\tilde{\bar{p}}_{\mathrm{fD,S}}(r_{\mathrm{wD}},n,\mathrm{s})+h_{\mathrm{D}}A_2\eta K_1(\eta r_{\mathrm{wD}})=\frac{1}{\mathrm{s}a_n} \tag{89}$$

From Eqs. (88) and (89), it is possible to cancel $\tilde{\bar{p}}_{\mathrm{fD,S}}(r_{\mathrm{wD}},n,\mathrm{s})$, resulting in:

$$\mathrm{s}C_{\mathrm{sD}}A_2\left[K_0(\eta r_{\mathrm{wD}})+Sh_{\mathrm{D}}\eta K_1(\eta r_{\mathrm{wD}})\right]+h_{\mathrm{D}}A_2\eta K_1(\eta r_{\mathrm{wD}})=\frac{1}{\mathrm{s}a_n} \tag{90}$$

From Eq. (90), we can obtain A_2 given by:

$$A_2=\frac{1}{\mathrm{s}a_n\left[\mathrm{s}C_{\mathrm{sD}}\left[K_0(\eta r_{\mathrm{wD}})+Sh_{\mathrm{D}}\eta K_1(\eta r_{\mathrm{wD}})\right]+h_{\mathrm{D}}\eta K_1(\eta r_{\mathrm{wD}})\right]} \tag{91}$$

By combining Eqs. (88) and (91), we arrive at:

$$\tilde{\bar{p}}_{\mathrm{fD,S}}(r_{\mathrm{wD}},n,\mathrm{s})=\frac{K_0(\eta r_{\mathrm{wD}})+Sh_{\mathrm{D}}\eta K_1(\eta r_{\mathrm{wD}})}{\mathrm{s}a_n\left[\mathrm{s}C_{\mathrm{sD}}\left[K_0(\eta r_{\mathrm{wD}})+Sh_{\mathrm{D}}\eta K_1(\eta r_{\mathrm{wD}})\right]+h_{\mathrm{D}}\eta K_1(\eta r_{\mathrm{wD}})\right]} \tag{92}$$

The inverse modified finite Fourier sine transform with respect to n is defined for $\tilde{\bar{p}}_{\mathrm{fD,S}}$ as follows:

$$\bar{p}_{\mathrm{fD,S}}(r_{\mathrm{wD}}, z_{\mathrm{D}}, \mathrm{s}) = \wp_n^{-1}\{\tilde{\bar{p}}_{\mathrm{fD,S}}(r_{\mathrm{wD}}, n, \mathrm{s})\} = \frac{2}{h_{\mathrm{oD}}} \sum_{n=1}^{+\infty} \tilde{\bar{p}}_{\mathrm{fD,S}}(r_{\mathrm{wD}}, n, \mathrm{s}) \sin(a_n z_{\mathrm{D}}) \quad 0 < z_{\mathrm{D}} < h_{\mathrm{oD}} \tag{93}$$

where $\wp_n^{-1}$ is the sign for the inverse modified finite Fourier sine transform with respect to n.

Equation (93) is a function of z_{D}. To obtain a dimensionless average fracture pressure in the Laplace domain along the dimensionless perforation interval of the well, Eq. (93) must be integrated with respect to z_{D} over the limits of the dimensionless perforation interval, h_{oD}-$h_{\mathrm{pD}} < z_{\mathrm{D}} < h_{\mathrm{oD}}$, divided by the dimensionless perforated interval of the oil zone, h_{pD}. Gerami and Pooladi-Darvish (2009) used the same approach to present a 2D mathematical model for a constant-rate drawdown test performed in a partially penetrated well completed in the free-gas zone of a hydrate-capped gas reservoir during the early time production. Therefore, by using this approach it is possible to write:

$$\bar{p}_{\mathrm{fD,S}}(r_{\mathrm{wD}}, \mathrm{s}) = \frac{1}{h_{\mathrm{pD}}} \int_{h_{\mathrm{oD}}-h_{\mathrm{pD}}}^{h_{\mathrm{oD}}} \bar{p}_{\mathrm{fD,S}}(r_{\mathrm{wD}}, z_{\mathrm{D}}, \mathrm{s}) dz_{\mathrm{D}} \tag{94}$$

By substituting Eq. (93) into Eq. (94), we get:

$$\bar{p}_{\mathrm{fD,S}}(r_{\mathrm{wD}}, \mathrm{s}) = \frac{1}{h_{\mathrm{pD}}} \int_{h_{\mathrm{oD}}-h_{\mathrm{pD}}}^{h_{\mathrm{oD}}} \frac{2}{h_{\mathrm{oD}}} \sum_{n=1}^{+\infty} \tilde{\bar{p}}_{\mathrm{fD,S}}(r_{\mathrm{wD}}, n, \mathrm{s}) \sin(a_n z_{\mathrm{D}}) dz_{\mathrm{D}} \tag{95}$$

Eq. (95) can be simplified as:

$$\bar{p}_{\mathrm{fD,S}}(r_{\mathrm{wD}}, \mathrm{s}) = \frac{2}{h_{\mathrm{oD}} h_{\mathrm{pD}}} \sum_{n=1}^{+\infty} \tilde{\bar{p}}_{\mathrm{fD}}, S(r_{\mathrm{wD}}, n, \mathrm{s}) \int_{h_{\mathrm{oD}}-h_{\mathrm{pD}}}^{h_{\mathrm{oD}}} \sin(a_n z_{\mathrm{D}}) dz_{\mathrm{D}} \tag{96}$$

The integral in Eq. (96) is calculated as:

$$\int_{h_{\mathrm{oD}}-h_{\mathrm{pD}}}^{h_{\mathrm{oD}}} \sin(a_n z_{\mathrm{D}}) dz_{\mathrm{D}} = \frac{2h_{\mathrm{oD}}}{(2n-1)\pi} \cos\left[\left(\frac{2n-1}{2}\right)(1-h_{\mathrm{D}})\,\pi\right] \tag{97}$$

By replacing Eq. (97) in Eq. (96), we have:

$$\bar{p}_{\mathrm{fD,S}}(r_{\mathrm{wD}}, \mathrm{s}) = \frac{1}{h_{\mathrm{pD}}} \sum_{n=1}^{+\infty} \left[\frac{4}{\pi(2n-1)} \cos\left[\left(\frac{2n-1}{2}\right)(1-h_{\mathrm{D}})\,\pi\right]\right] \tilde{\bar{p}}_{\mathrm{fD,S}}(r_{\mathrm{wD}}, n, \mathrm{s}) \tag{98}$$

By substituting Eq. (92) into Eq. (98), it is possible to arrive at:

$$\bar{p}_{\mathrm{fD,S}}(r_{\mathrm{wD}}, \mathrm{s}) = \frac{1}{h_{\mathrm{pD}}} \sum_{n=1}^{+\infty} \left[\frac{\frac{4}{\pi(2n-1)}\left[K_0(\eta r_{\mathrm{wD}}) + Sh_{\mathrm{D}}\eta K_1(\eta r_{\mathrm{wD}})\right] \cos\left[\left(\frac{2n-1}{2}\right)(1-h_{\mathrm{D}})\,\pi\right]}{\mathrm{s}a_n\left[sC_{\mathrm{sD}}\left[K_0(\eta r_{\mathrm{wD}}) + Sh_{\mathrm{D}}\eta K_1(\eta r_{\mathrm{wD}})\right] + h_{\mathrm{D}}\eta K_1(\eta r_{\mathrm{wD}})\right]}\right] \tag{99}$$

Eq. (99) is only a function of "s". Therefore, Eq. (99) can be written as below:

$$\bar{p}_{\mathrm{fD,S}}(\mathrm{s}) = \frac{1}{h_{\mathrm{pD}}} \sum_{n=1}^{+\infty} \left[\frac{\frac{4}{\pi(2n-1)} \left[K_0(\eta r_{\mathrm{wD}}) + Sh_{\mathrm{D}} \eta K_1(\eta r_{\mathrm{wD}})\right] \cos\left[\left(\frac{2n-1}{2}\right)(1-h_{\mathrm{D}})\,\pi\right]}{\mathrm{s} a_n \left[\mathrm{s} C_{\mathrm{sD}} \left[K_0(\eta r_{\mathrm{wD}}) + Sh_{\mathrm{D}} \eta K_1(\eta r_{\mathrm{wD}})\right] + h_{\mathrm{D}} \eta K_1(\eta r_{\mathrm{wD}})\right]} \right] \tag{100}$$

Equation (100) shows the dimensionless average pressure at the wellbore ($r_{\mathrm{D}} = r_{\mathrm{wD}}$) in the Laplace domain. Therefore, it is possible to replace $\bar{p}_{\mathrm{fD,S}}$ by $\bar{p}_{\mathrm{wD}}$ in Eq. (100), resulting in:

$$\bar{p}_{\mathrm{wD}}(\mathrm{s}) = \frac{1}{h_{\mathrm{pD}}} \sum_{n=1}^{+\infty} \left[\frac{\frac{4}{\pi(2n-1)} \left[K_0(\eta r_{\mathrm{wD}}) + Sh_{\mathrm{D}} \eta K_1(\eta r_{\mathrm{wD}})\right] \cos\left[\left(\frac{2n-1}{2}\right)(1-h_{\mathrm{D}})\,\pi\right]}{\mathrm{s} a_n \left[\mathrm{s} C_{\mathrm{sD}} \left[K_0(\eta r_{\mathrm{wD}}) + Sh_{\mathrm{D}} \eta K_1(\eta r_{\mathrm{wD}})\right] + h_{\mathrm{D}} \eta K_1(\eta r_{\mathrm{wD}})\right]} \right] \tag{101}$$

By applying a numerical Laplace inversion method (Hassanzadeh and Pooladi-Darvish 2007; Mashayekhizadeh et al. 2011) for Eq. (101), the dimensionless average pressure response of the well (p_{wD}) in the oil zone of an infinite-acting double-porosity reservoir, including wellbore storage and skin effects, can be obtained as follows:

$$p_{\mathrm{wD}}(t_{\mathrm{D}}) = \ell_{\mathrm{s}}^{-1} \left\{ \frac{1}{h_{\mathrm{pD}}} \sum_{n=1}^{+\infty} \left[\frac{\frac{4}{\pi(2n-1)} \left[K_0(\eta r_{\mathrm{wD}}) + Sh_{\mathrm{D}} \eta K_1(\eta r_{\mathrm{wD}})\right] \cos\left[\left(\frac{2n-1}{2}\right)(1-h_{\mathrm{D}})\,\pi\right]}{\mathrm{s} a_n \left[s C_{\mathrm{sD}} \left[K_0(\eta r_{\mathrm{wD}}) + Sh_{\mathrm{D}} \eta K_1(\eta r_{\mathrm{wD}})\right] + h_{\mathrm{D}} \eta K_1(\eta r_{\mathrm{wD}})\right]} \right] \right\} \tag{102}$$

where

$$p_{\mathrm{wD}}(t_{\mathrm{D}}) = \ell_{\mathrm{s}}^{-1}\{\bar{p}_{\mathrm{wD}}(\mathrm{s})\} \tag{103}$$

The time derivative of the dimensionless average pressure can be applied to analyze and interpret the well test data more precisely. After replacing p_{fD} by p_{wD} and $\bar{p}_{\mathrm{fD}}$ by $\bar{p}_{\mathrm{wD}}$ in Eq. (51), we have:

$$\ell_{t_{\mathrm{D}}} \left\{ \frac{\mathrm{d} p_{\mathrm{wD}}(t_{\mathrm{D}})}{\mathrm{d} t_{\mathrm{D}}} \right\} = \mathrm{s} \bar{p}_{\mathrm{wD}}(\mathrm{s}) \tag{104}$$

Eq. (104) can be written as follows:

$$\frac{\mathrm{d} p_{\mathrm{wD}}(t_{\mathrm{D}})}{\mathrm{d} t_{\mathrm{D}}} = \ell_{\mathrm{s}}^{-1}\{s \bar{p}_{\mathrm{wD}}(\mathrm{s})\} \tag{105}$$

To obtain $dp_{\mathrm{wD}}/dt_{\mathrm{D}}$, we need to multiply $\bar{p}_{\mathrm{wD}}(\mathrm{s})$ from Eq. (101) by "s" and then take the Laplace inverse. However, in well testing, $\mathrm{d}p_{\mathrm{wD}}/\mathrm{d}\ln t_{\mathrm{D}}$ is used as the derivative of the dimensionless average pressure response of the well. $\mathrm{d}p_{\mathrm{wD}}/\mathrm{d}\ln t_{\mathrm{D}}$ can be simplified as below:

$$\frac{\mathrm{d} p_{\mathrm{wD}}(t_{\mathrm{D}})}{\mathrm{d} \ln t_{\mathrm{D}}} = t_{\mathrm{D}} \frac{\mathrm{d} p_{\mathrm{wD}}(t_{\mathrm{D}})}{\mathrm{d} t_{\mathrm{D}}} \tag{106}$$

By substituting Eq. (105) into Eq. (106), it is possible to find $\mathrm{d}p_{\mathrm{wD}}/\mathrm{d}\ln t_{\mathrm{D}}$ as follows:

$$\frac{\mathrm{d} p_{\mathrm{wD}}(t_{\mathrm{D}})}{\mathrm{d} \ln t_{\mathrm{D}}} = t_{\mathrm{D}} \ell_{\mathrm{s}}^{-1}\{\mathrm{s} \bar{p}_{\mathrm{wD}}(\mathrm{s})\} \tag{107}$$

In this work, the Stehfest (1970) method is applied for numerical Laplace inversion.

References

Abdassah, D., Ershaghi, I.: Triple-porosity systems for representing naturally fractured reservoirs. SPE Form. Eval. **1**(2), 113–127 (1986)

Agarwal, R.G., Al-Hussainy, R.: An investigation of wellbore storage and skin effect in unsteady liquid flow: I. Analytical treatment. Soc. Pet. Eng. J. **10**(3), 279–290 (1970)

Al-Bemani, A.S., Ershaghi, I.: Gas-cap effects in pressure-transient response of naturally fractured reservoirs. SPE Form. Eval. **12**(1), 40–46 (1997)

Barenblatt, G.I., Zheltov, Y.P., Kochina, I.N.: Basic concepts in the theory of seepage of homogeneous liquids in fissured rocks. J. Appl. Math. Mech. **24**(5), 852–864 (1960)

Bilhartz, Jr H.L., Ramey, Jr H.J.: The combined effects of storage, skin, and partial penetration on well test analysis. In: Paper SPE 6753, Presented at the SPE Annual Fall Technical Conference and Exhibition, Denver, Colorado (1977)

Biryukov, D., Kuchuk, F.J.: Transient pressure behavior of reservoirs with discrete conductive faults and fractures. Transp. Porous Med. **95**(1), 239–268 (2012)

Bourdet, D., Gringarten, A.C.: Determination of fissure volume and block size in fractured reservoirs by type-curve analysis. In: Paper SPE 9293, Presented at the SPE Annual Technical Conference and Exhibition, Dallas (1980)

Buhidma, I.M., Raghavan, R.: Transient pressure behavior of partially penetrating wells subject to bottomwater drive. J. Pet. Technol. **32**(7), 1251–1261 (1980)

Bui, T.D., Mamora, D.D., Lee, W.J.: Transient pressure analysis for partially penetrating wells in naturally fractured reservoirs. In: Paper SPE 60289, Presented at the SPE Rocky Mountain Regional/Low Permeability Reservoirs Symposium and Exhibition, Denver (2000)

Cassiani, G., Kabala, Z.J.: Flowing partially penetrating well: solution to a mixed-type boundary value problem. Adv. Water Resour. **23**(1), 59–68 (1999)

Chen, Z.X.: Transient flow of slightly compressible fluids through double-porosity, double-permeability systems: a state-of-the-art review. Transp. Porous Media **4**(2), 147–184 (1989)

Chen, F.F., Jia, Y.L., Zhang, F.X.: Partial perforated filtration model and the typical curve of well test for dual media. Petroleum Geol. Oilfield Dev. Daqing **27**(6), 87–90 (2008)

Chen, H.Y., Poston, S.W., Raghavan, R.: An application of the product solution principle for instantaneous source and Green's functions. SPE Form. Eval. **6**(2), 161–167 (1991)

Chu, W.C., Chen, J.C., Reynolds, A.C., Raghavan, R.: On the analysis of well test data influenced by wellbore storage, skin, and bottomwater drive. J. Pet. Technol. **36**(11), 1991–2001 (1984)

Da Prat, G.: Well Test Analysis for Fractured Reservoir Evaluation. Elsevier, New York (1990)

de Swaan, O.A.: Analytic solutions for determining naturally fractured reservoir properties by well testing. Soc. Pet. Eng. J. **16**(3), 117–122 (1976)

De Smedt, F.: Analytical solution for constant-rate pumping test in fissured porous media with double-porosity behaviour. Transp. Porous Media **88**(3), 479–489 (2011)

Dougherty, D.E., Babu, D.K.: Flow to a partially penetrating well in a double porosity reservoir. Water Resour. Res. **20**(8), 1116–1122 (1984)

Earlougher Jr, R.C., Kersch, K.M.: Analysis of short-time transient test data by type-curve matching. J. Pet. Technol. **26**(7), 793–800 (1974)

Fuentes-Cruz, G., Camacho-Velázquez, R., Vásquez-Cruz, M.: Pressure transient and decline curve behaviors for partially penetrating wells completed in naturally fractured–vuggy reservoirs. In: Paper SPE 92116, presented at the SPE International Petroleum Conference in Mexico, Puebla (2004)

Gerami, S., Pooladi-Darvish, M.: An early-time model for drawdown testing of a hydrate-capped gas reservoir. SPE Reserv. Eval. Eng. **12**(4), 595–609 (2009)

Gringarten, A.C., Ramey Jr, H.J.: The use of source and Green's functions in solving unsteady-flow problems in reservoirs. Soc. Pet. Eng. J. **13**(5), 285–296 (1973)

Hamm, S.Y., Bidaux, P.: Dual-porosity fractal models for transient flow analysis in fissured rocks. Water Resour. Res. **32**(9), 2733–2745 (1996)

Hassanzadeh, H., Pooladi-Darvish, M.: Comparison of different numerical Laplace inversion methods for engineering applications. Appl. Math. Comput. **189**(2), 1966–1981 (2007)

Hassanzadeh, H., Pooladi-Darvish, M., Atabay, S.: Shape factor in the drawdown solution for well testing of dual-porosity systems. Adv. Water Resour. **32**(11), 1652–1663 (2009)

Hawkins Jr, M.F.: A note on the skin effect. J. Pet. Technol. **8**(12), 65–66 (1956)

Houzé, O., Viturat, D., Fjaere, O.S.: Dynamic Flow Analysis. KAPPA Corporation, Paris (2007)

Jalali, Y., Ershaghi, I.: A unified type curve approach for pressure transient analysis of naturally fractured reservoirs. In: Paper SPE 16778, Presented at the SPE Annual Technical Conference and Exhibition, Dallas (1987)

Jia, Y.L., Fan, X.Y., Nie, R.S., Huang, Q.H., Jia, Y.L.: Flow modeling of well test analysis for porous–vuggy carbonate reservoirs. Transp. Porous Media **97**(2), 253–279 (2013)
Kabala, Z.J.: Sensitivity analysis of a pumping test on a well with wellbore storage and skin. Adv. Water Resour. **24**(5), 483–504 (2001)
Kazemi, H.: Pressure transient analysis of naturally fractured reservoirs with uniform fracture distribution. Soc. Pet. Eng. J. **9**(4), 451–462 (1969)
Lods, G., Gouze, P.: WTFM, software for well test analysis in fractured media combining fractional flow with double porosity and leakance approaches. Comput. Geosci. **30**, 937–947 (2004)
Mashayekhizadeh, V., Dejam, M., Ghazanfari, M.H.: The application of numerical Laplace inversion methods for type curve development in well testing: a comparative study. Petrol. Sci. Technol. **29**(7), 695–707 (2011)
Moench, A.F.: Double-porosity models for a fissured groundwater reservoir with fracture skin. Water Resour. Res. **20**(7), 831–846 (1984)
Moench, A.F.: Transient flow to a large-diameter well in an aquifer with storative semiconfining layers. Water Resour. Res. **21**(8), 1121–1131 (1985)
Najurieta, H.L.: A theory for pressure transient analysis in naturally fractured reservoirs. J. Pet. Technol. **32**(7), 1241–1250 (1980)
Nie, R.S., Meng, Y.F., Jia, Y.L., Zhang, F.X., Yang, X.T., Niu, X.N.: Dual porosity and dual permeability modeling of horizontal well in naturally fractured reservoir. Transp. Porous Media **92**(1), 213–235 (2012)
Ozkan, E., Ohaeri, U., Raghavan, R.: Unsteady flow to a well produced at a constant pressure in a fractured reservoir. SPE Form. Eval. **2**(2), 186–200 (1987)
Ozkan, E., Raghavan, R.: New solutions for well-test-analysis problems: part 1: analytical considerations. SPE Form. Eval. **6**(3), 359–368 (1991a)
Ozkan, E., Raghavan, R.: New solutions for well-test-analysis problems: part 2: computational considerations and applications. SPE Form. Eval **6**(3), 369–378 (1991b)
Pasandi, M., Samani, N., Barry, D.A.: Effect of wellbore storage and finite thickness skin on flow to a partially penetrating well in a phreatic aquifer. Adv. Water Resour. **31**(2), 383–398 (2008)
Peaceman, D.W.: Convection in fractured reservoirs: the effect of matrix-fissure transfer on the instability of a density inversion in a vertical fissure. Soc. Pet. Eng. J. **16**(5), 269–280 (1976)
Ramey Jr, H.J., Agarwal, R.G.: Annulus unloading rates as influenced by wellbore storage and skin effect. Soc. Pet. Eng. J. **12**(5), 453–462 (1972)
Sabet, M.A.: Well Test Analysis. Gulf Publishing Company, Houston (1991)
Saidi, A.M.: Reservoir Engineering of Fractured Reservoirs, Total edn. Press, Paris (1987)
Saidi, A.M.: Simulation of naturally fractured reservoirs. In: Paper SPE 12270, Presented at the SPE Reservoir Simulation Symposium, San Francisco (1983)
Sandal, H.M., Horne, R.N., Ramey, Jr H.J., Williamson, J.W.: Interference testing with wellbore storage and skin effects at the produced well. In: Paper SPE 7454, Presented at the SPE Annual Fall Technical Conference and Exhibition, Houston (1978)
Sethi, R.: A dual-well step drawdown method for the estimation of linear and non-linear flow parameters and wellbore skin factor in confined aquifer systems. J. Hydrol. **400**, 187–194 (2011)
Serra, K., Reynolds, A.C., Raghavan, R.: New pressure transient analysis methods for naturally fractured reservoirs. J. Pet. Technol. **35**(12), 2271–2283 (1983)
Slimani, K., Tiab, D.: Pressure transient analysis of partially penetrating wells in a naturally fractured reservoir. J. Can. Pet. Technol. **47**(5), 63–69 (2008)
Stehfest, H.: Algorithm 368: numerical inversion of Laplace transform. Commun. Assoc. Comput. Math. **13**(1), 47–49 (1970)
Stewart, G., Asharsobbi, F.: Well test interpretation for naturally fractured reservoirs. In: Paper SPE 18173, Presented at the SPE Annual Technical Conference and Exhibition, Houston (1988)
Streltsova, T.D.: Pressure drawdown in a well with limited flow entry. J. Pet. Technol. **31**(11), 1469–1476 (1979)
Streltsova, T.D.: Pressure transient analysis for afterflow-dominated wells producing from a reservoir with a gas cap. J. Pet. Technol. **33**(4), 743–754 (1981)
Streltsova, T.D.: Well pressure behavior of a naturally fractured reservoir. Soc. Pet. Eng. J. **23**(5), 769–780 (1983)
Tariq, S.M., Ramey, Jr H.J.: Drawdown behavior of a well with storage and skin effect communicating with layers of different radii and other characteristics. In: Paper SPE 7453, Presented at the SPE Annual Fall Technical Conference and Exhibition, Houston (1978)
van Everdingen, A.F.: The skin effect and its influence on the productive capacity of a well. Petroleum Trans. AIME **198**, 171–176 (1953)

van Everdingen, A.F., Hurst, W.: The application of the Laplace transformation to flow problems in reservoirs. Petroleum Trans. AIME **186**, 305–324 (1949)
Warren, J.E., Root, P.J.: The behavior of naturally fractured reservoirs. Soc. Pet. Eng. J. **3**(3), 245–255 (1963)
Wattenbarger, R.A., Ramey Jr, H.J.: An investigation of wellbore storage and skin effect in unsteady liquid flow: II. finite difference treatment. Soc. Pet. Eng. J **10**(3), 291–297 (1970)
Yang, Y.J., Gates, T.M.: Wellbore skin effect in slug-test data analysis for low-permeability geologic materials. Ground Water **35**(6), 931–937 (1997)
Yao, Y., Wu, Y.S., Zhang, R.: The transient flow analysis of fluid in a fractal, double-porosity reservoir. Transp. Porous Media **94**(1), 175–187 (2012)
Zimmerman, R.W., Chen, G., Hadgu, T., Bodvarsson, G.S.: A numerical dual-porosity model with semianalytical treatment of fracture/matrix flow. Water Resour. Res. **29**(7), 2127–2137 (1993)